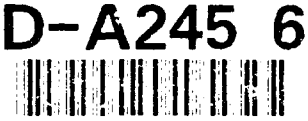

2

A TRIDENT SCHOLAR PROJECT REPORT

NO. 182

"DEVELOPMENT OF ION BEAM ANALYSIS TECHNIQUES FOR ARCHEOLOGICAL RESEARCH"

"Original contains color plates: All DTIC reproductions will be in black and white"

UNITED STATES NAVAL ACADEMY
ANNAPOLIS, MARYLAND

DISCLAIMER NOTICE

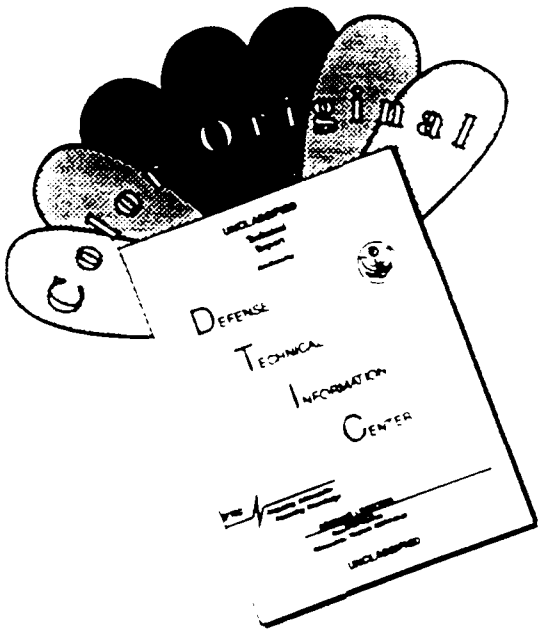

THIS DOCUMENT IS BEST QUALITY AVAILABLE. THE COPY FURNISHED TO DTIC CONTAINED A SIGNIFICANT NUMBER OF COLOR PAGES WHICH DO NOT REPRODUCE LEGIBLY ON BLACK AND WHITE MICROFICHE.

"DEVELOPMENT OF ION BEAM ANALYSIS TECHNIQUES FOR ARCHEOLOGICAL RESEARCH"

A Trident Scholar Project Report

by

Midshipman William David Kulp, III, Class of 1991

U. S. Naval Academy

Annapolis, Maryland

Francis D Correll

Adviser: Associate Professor Francis D. Correll
Physics Department

James R Huddle

Adviser: Assistant Professor James R. Huddle
Physics Department

Accepted for Trident Scholar Committee

Francis D Correll

Chair

13 May 1991

Date

REPORT DOCUMENTATION PAGE

Form Approved
OMB No. 0704-0188

1. AGENCY USE ONLY (Leave blank)	2. REPORT DATE	3. REPORT TYPE AND DATES COVERED
	13 May 1991	Final 1990/91

4. TITLE AND SUBTITLE

DEVELOPMENT OF ION BEAM ANALYSIS TECHNIQUES FOR ARCHEOLOGICAL RESEARCH

5. FUNDING NUMBERS

6. AUTHOR(S)

William David Kulp, III

7. PERFORMING ORGANIZATION NAME(S) AND ADDRESS(ES)

U.S. Naval Academy, Annapolis, MD

8. PERFORMING ORGANIZATION REPORT NUMBER

U.S.N.A. - TSPR; 182 (1991)

9. SPONSORING/MONITORING AGENCY NAME(S) AND ADDRESS(ES)

10. SPONSORING/MONITORING AGENCY REPORT NUMBER

11. SUPPLEMENTARY NOTES

Accepted by the U.S. Trident Scholar Committee.

12a. DISTRIBUTION/AVAILABILITY STATEMENT

This document has been approved for public release; its distribution is UNLIMITED.

12b. DISTRIBUTION CODE

13. ABSTRACT (Maximum 200 words)

Particle-induced x-ray emission (PIXE) has been investigated as a technique for studying prehistoric stone tools collected from sites in southern Maryland by archeologists at the Maryland Historical Trust. Experimental apparatus, including a sample positioner, x-ray detector, x-ray filters, and electronics have been designed, assembled, or optimized for the project. Data analysis software has been obtained, installed, and modified as needed. The elemental compositions of 51 rhyolite tools have been measured using in-air PIXE, and the data have been subjected to a statistical analysis to reveal similarities between the compositions of different tools. The results of this analysis have been interpreted in terms of several models of prehistoric trade.

14. SUBJECT TERMS

Proton-induced X-ray emission
Ion bombardment
Archaeological physics
Rhyolite

15. NUMBER OF PAGES

60

16. PRICE CODE

17. SECURITY CLASSIFICATION OF REPORT	18. SECURITY CLASSIFICATION OF THIS PAGE	19. SECURITY CLASSIFICATION OF ABSTRACT	20. LIMITATION OF ABSTRACT
UNCLASSIFIED	UNCLASSIFIED	UNCLASSIFIED	

ABSTRACT

Particle-induced x-ray emission (PIXE) has been investigated as a technique for studying prehistoric stone tools collected from sites in southern Maryland by archeologists at the Maryland Historical Trust. Experimental apparatus, including a sample positioner, x-ray detector, x-ray filters, and electronics have been designed, assembled, or optimized for the project. Data analysis software has been obtained, installed, and modified as needed. The elemental compositions of 51 rhyolite tools have been measured using in-air PIXE, and the data have been subjected to a statistical analysis to reveal similarities between the compositions of different tools. The results of this analysis have been interpreted in terms of several models of prehistoric trade.

ACKNOWLEDGMENTS

I would like to recognize and thank the individuals whose assistance and guidance made this project possible.

Dr. Stuart Reeve, Assistant Administrator of Research for the Jefferson Patterson Park and Museum, deserves special thanks for his insight and archeological tutelage, not to mention rhyolites, that provided the necessary background for this project. Assistant Professor Jeffrey Vanhoy saved immeasurable amounts of analysis time by bringing the micro-VAX on-line and by providing useful debugging suggestions for the modified PIXAN code. Mr. Charlie Hollaway, the physics shop machinist, provided the finely-crafted equipment necessary for the implementation of the Si(Li) detector and target holder. Dr. Charles Swann provided timely advice concerning the use of PIXAN and the selection of an absorber. Essential to the success of the project, however, were my two advisers: Assistant Professor J. R. Huddle, whose help and humor in the laboratory made data collection interesting and memorable, and Associate Professor F. D. Correll whose heroic devotion of time, effort, and faith deserves my utmost appreciation and gratitude.

I will not forget the lessons learned or the memories made in our hot little laboratory in the basement.

Thanks to everyone,

Dave Kulp

TABLE OF CONTENTS

1. INTRODUCTION: ION BEAMS AND ARCHEOLOGY

1.1. THE NAVAL ACADEMY TANDEM ACCELERATOR LABORATORY

NATALY, the Naval Academy Tandem Accelerator Laboratory, is a new facility for ion beam analysis which became operational in 1989. At the heart of the laboratory is a National Electrostatics Corporation Pelletron™ 5SDH Tandem Electrostatic Accelerator capable of accelerating either protons or alpha particles for use in class laboratory exercises or materials analysis research. The use of ion beams in materials analysis has grown in popularity and potential over the last two decades due to recognition of the advantages and many applications of this method.

Ion beam analysis (IBA) permits rapid, nondestructive elemental analysis of many different kinds of materials. Applications of IBA include elemental analysis of synthetic materials, such as superconductors and composite materials, artwork, biological and geological samples, and archeological artifacts. In this last discipline, the use of IBA techniques in the study of archeological artifacts, research has progressed rapidly in recent years, due to the increased availability of small accelerators and the real applications of trace elemental analysis in archeological studies.

Trace elemental analyses may be used to study a variety of topics in archeology . Recent applications include classification of silver coins [1], examining the compounds used to produce different colored glazes in ancient Egypt [2], tracing environmental changes over time through analysis of mussel shells [3], and exploring the geographic origins of artifacts in order to track migration and trade patterns in prehistoric times [4]. In each case, the trace elemental composition of the materials studied has provided clues necessary for unlocking secrets buried beneath the earth and obscured by time.

1.2. THE MARYLAND HISTORICAL TRUST ARCHEOLOGY PROJECT

An archeological survey of southern Maryland was initiated in 1989 by the Maryland Historical Trust in order to locate territories inhabited by colonial ancestors and prehistoric peoples in that area before such sites were destroyed by widespread development [5]. Of special interest was the lower estuary of the Patuxent River, an area inhabited by prehistoric Native Americans for more than 9000 years and the site of one of the earliest European settlements on this continent. One site, Patuxent Point, which is located along the Patuxent River near the Chesapeake Bay, yielded a remarkably large number of rhyolite* stone tools dating from the Middle Woodland Selby Bay period (200-900 AD). Although rhyolite tools were also used during other periods and in other areas, this particular site was of interest because the Middle Woodland Selby Bay phase was the period when rhyolite tools were used most intensively throughout southern Maryland and the Middle Atlantic region [6].

The discovery of large numbers of tools fashioned from rhyolites in this region is unusual and interesting for several reasons. In the first place, simply finding rhyolite in southern Maryland is remarkable because the nearest source is located in the mountains of the Blue Ridge Province of Maryland, over 200 kilometers distant [7, 8]. Further, the discovery of such a large number of stone tools, a total of over 800 artifacts in one place, indicates the development of sedentism and the settlement of the area [5]. In addition, approximately 90% of all the stone tools found and attributed to this era were rhyolite, while the usage of rhyolites in the epochs immediately before and after the Selby Bay Phase show a maximum of 10% of the tools found were rhyolite. Other, more readily available, materials such as quartz, quartzite, and argillite are better knapping* materials suitable for stone tool manufacture, raising the question of why rhyolites were used almost exclusively for 700 years when there were ample, nearby, sources of better stones. In addition to the

* In this paper, an asterisk indicates words defined in the Glossary.

questions surrounding the stones themselves, however, the social implications of their presence and distribution here are quite important.

Previous studies found rhyolite projectile points far from the sources in northern Maryland and western Pennsylvania, but were inconclusive concerning their transport and origins [9, 10]. Popular models of trade and exchange for the Woodland period include broad-based exchange, focused exchange, and limited exchange [5, 9]. Broad-based exchange is indicative of a less-developed society, where the participants in the trade are on relatively equal terms and trade for subsistence or kinship reasons. Focused trade indicates the presence of a chieftain or other single leader of political prominence who is able to focus trade to his own needs and hoard what is considered important. Limited exchange describes a situation in which social groups would send task groups out to collect rocks for a whole community. The limited exchange model was proposed by Stewart, who noted that food resources in the areas around rhyolite formations were so limited that "the most effective strategy for rhyolite-craving groups would have been to grab the rock and run" [7].

One way to choose between the models would be to examine how well the sources of rhyolite matched with the site where the stones were found. For example, in the case where the stones varied a great deal among sites, and no specific site could be matched with a particular quarry or source, this could be interpreted as evidence of the broad-based exchange model. Evidence indicative of focused trade would be the appearance of several types of stone at one site, while nearby sites showed signs of only one source. Lastly, a site which appeared to contain stones from a solitary source would be a good indication of task groups being sent into the mountains to collect raw materials and return to the larger bands on the Piedmont, which is evidence of the limited exchange model.

1.3. THE PRESENT PROJECT

Dr. Stuart Reeve of the Jefferson Patterson Park and Museum proposed studying the rhyolite stone tools found in southern Maryland using trace element analysis [11]. The goals of this analysis were to determine the sources of these projectile points and challenge the several models of trade and exchange in prehistoric times. The recent availability of NATALY and the interesting questions posed by studying rhyolites, a material never before examined using IBA techniques, made the use of IBA attractive both for archeologists and physicists.

Three IBA techniques were considered promising for the study of these points: Particle-Induced X-Ray Emission (PIXE), Rutherford Backscattering Spectroscopy (RBS), and Particle-Induced Gamma-Ray Emission (PIGE). The first and last techniques mentioned, PIXE and PIGE, are methods in which photons emitted from irradiated targets are collected and analyzed, whereas RBS analyzes the energy of charged particles scattered from impact with the target. Because each technique requires some degree of expertise and specialization in order to achieve the maximum degree of precision for a specific material, refinement of the techniques mentioned would be essential for a detailed analysis of the rhyolites.

The purpose of this project was to select an IBA method most suited for the study of rhyolites and to develop the techniques necessary to ensure that accurate elemental concentrations could be measured. An associated goal was to acquire a database of the trace elemental composition of artifacts provided for analysis by the Maryland Historical Trust. Achievement of both goals would provide information that would assist in determining the origins of rhyolites found in southern Maryland and in evaluating present models for prehistoric trade and exchange.

1.4. THE SAMPLES

Fifty-five projectile points found in the Patuxent River estuary, displayed in Figure 1, and in associated areas of the Potomac and Susquehanna River systems were provided for analysis in this study. The majority of the samples, as indicated in Table I, were from the Patuxent River estuary. Patuxent Point and sites along the Patuxent River were favored numerically in an effort to evaluate the accuracy of a model of limited exchange. If the theory of limited exchange proved to be true, a smaller site distribution would be useful in determining the size of groups which collected their own rhyolite rocks. Conversely, samples from the Potomac and Susquehanna Rivers were included in order to gauge the extent of broad-based or focused trade and exchange through the analysis of sites relatively far removed from one another.

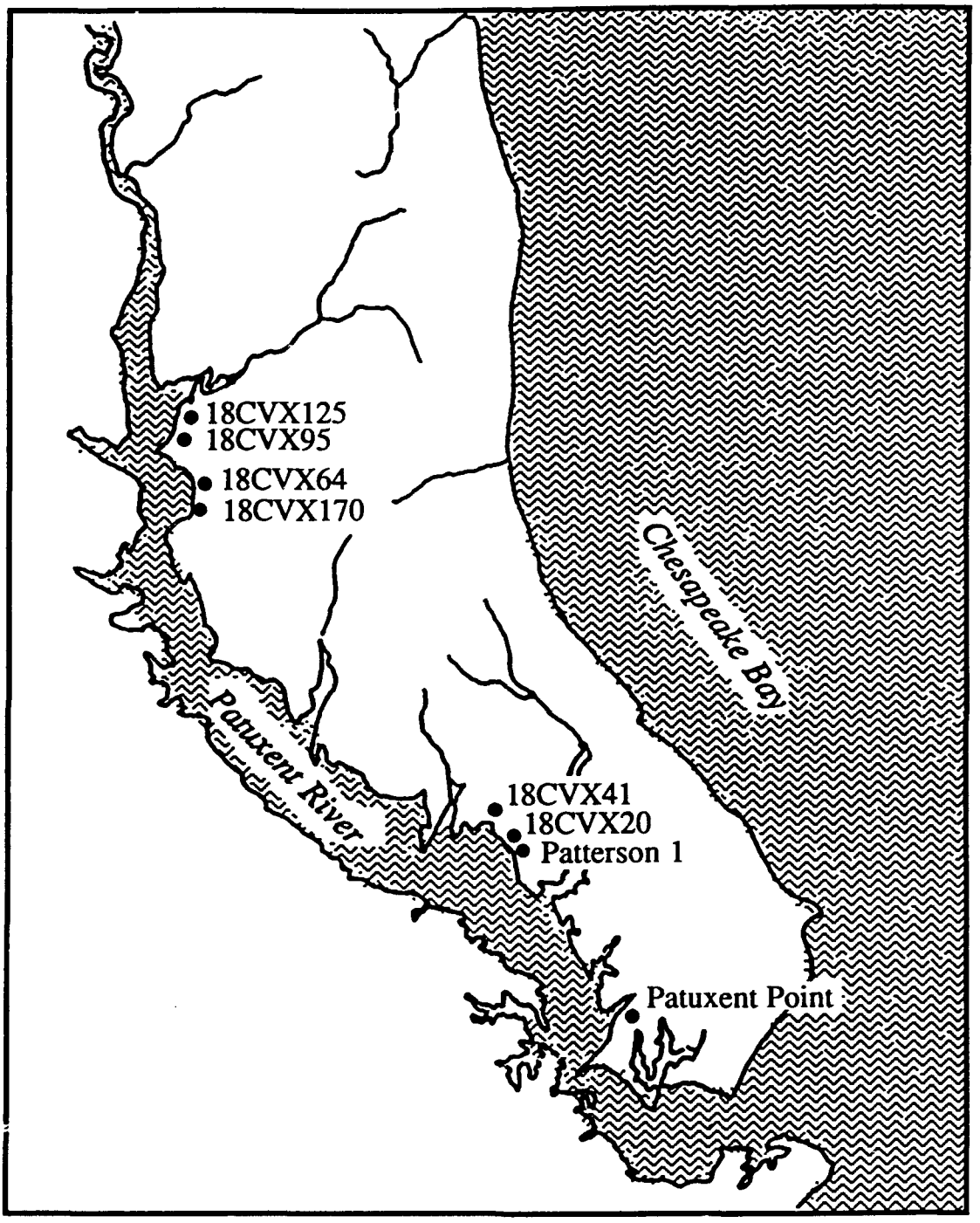

Figure 1. Some Middle Woodland sites of the lower Patuxent River from which the rhyolite stone points in this study were obtained.

Table I. Inventory of rhyolite points used in this study.

Key: SEQ. NO. = arbitrary sequence number, used to identify samples; SITE = general collection area; PROVENIENCE = location within the site; MATERIAL = rhyolite grade, assigned on the basis of visual examination.

SEQ. NO.	SITE	PROVENIENCE	MATERIAL	RIVER SYSTEM
1	18CV271	SC1906	5	Patuxent River
2	18CV271	Fea 2107	2	Patuxent River
3	18CV271	Fea 2204	2	Patuxent River
4	18CV271	Fea 2406	2	Patuxent River
5	18CV271	SC 2509	2	Patuxent River
6	18CV271	Fea 2608H	2	Patuxent River
8	18CV271	SC 2807	3	Patuxent River
9	18CV271	SC 2811	1	Patuxent River
10	18CV271	SC 2918	6	Patuxent River
11	18CV271	SC 3113	3	Patuxent River
12	18CV271	SC 4326	3	Patuxent River
13	18CV271	SC 4614	3	Patuxent River
14	18CV271	SC 4715	4?	Patuxent River
15	18CV271	SC 4720	3	Patuxent River
16	18CV271	SC 4925	3	Patuxent River
17	18CV271	SC 5021	2	Patuxent River
18	18CV278	Area A V	3	Patuxent River
19	18CV278	Area A II	3	Patuxent River
20	18CV261	Area B IV	3	Patuxent River
21	18CV271	Area D IX	2	Patuxent River
22	18CV271	Area D XIII	3	Patuxent River
23	18CV271	Area D XVI	2	Patuxent River
24	18CV272	Fea 3	2	Patuxent River
25	18CV65	Fea 303G	1	Patuxent River
27	18CV65	Fea 303H	1	Patuxent River
29	18CV65	M-1/1	3	Patuxent River
30	18CVX20	1B	5	Patuxent River
31	18CVX20	1D	5	Patuxent River
32	18CVX41	2J	3	Patuxent River
33	18CVX41	2N	3	Patuxent River
34	18CVX170	0D	5	Patuxent River
35	18CVX95	19	3	Patuxent River
36	18CVX95	31	3	Patuxent River
37	18CVX95	33	5	Patuxent River
38	18CVX125	5	3	Patuxent River
39	18CVX64	20	3	Patuxent River
40	90.4.20	Selden Island	3	Potomac River
41	90.4.21	Harrison Island	3	Potomac River
42	90.4.22	Mason Island	2	Potomac River
43	90.4.23	Mason Island B	2	Potomac River
44	90.4.24	Mason Island B	2	Potomac River
45	90.4.25	Mason Island	2	Potomac River
46	90.4.26	Mason Island	3	Potomac River
48	85.5.20	Unknown	1	Susquehanna River
49	85.5.21	Unknown	3	Susquehanna River
50	85.5.22	Unknown	1	Susquehanna River
51	85.5.23	Unknown	1	Susquehanna River
52	85.5.24	Unknown	3	Susquehanna River
53	85.5.25	Unknown	1	Susquehanna River
54	85.5.26	Unknown	3	Susquehanna River
55	85.5.27	Unknown	3	Susquehanna River

2. ION BEAM ANALYSIS

2.1. OVERVIEW

Ion beam analysis (IBA) techniques were considered for use in the study of the stone tools for several reasons. Because all IBA techniques are essentially nondestructive, analysis of the stone tools would not harm the artifacts in any way, and would allow for study in their original state as well as for later analysis by other methods. Multielemental detection capability, another trademark of IBA techniques, meant that one analysis method would simultaneously provide information on many of the elements present in the sample. Because most IBA techniques are also rapid, a large number of samples could be included in the study. Finally, due to the flexibility of the NATALY system which allows for the acceleration of either protons or helium ions, several different techniques were considered for use in this study.

2.2. ION BEAM ANALYSIS METHODS

A description of each IBA method, including particles used, experimental setup and spectra developed follows.

2.2.1. PARTICLE-INDUCED X-RAY EMISSION (PIXE)

Particle-induced X-ray emission (PIXE) is an analytical method of determining trace element compositions of samples using the x-ray spectra emitted when the samples are irradiated by a beam of high-energy particles. This method involves accelerating ions, usually protons, to a high energy and allowing the ion beam to strike a target and induce the atomic processes of ionization and characteristic x-ray emission. Because each element has its own x-ray energy "fingerprint," concentration analysis is possible in principle by simply counting the number of X rays of specific energies emitted by a target. This is

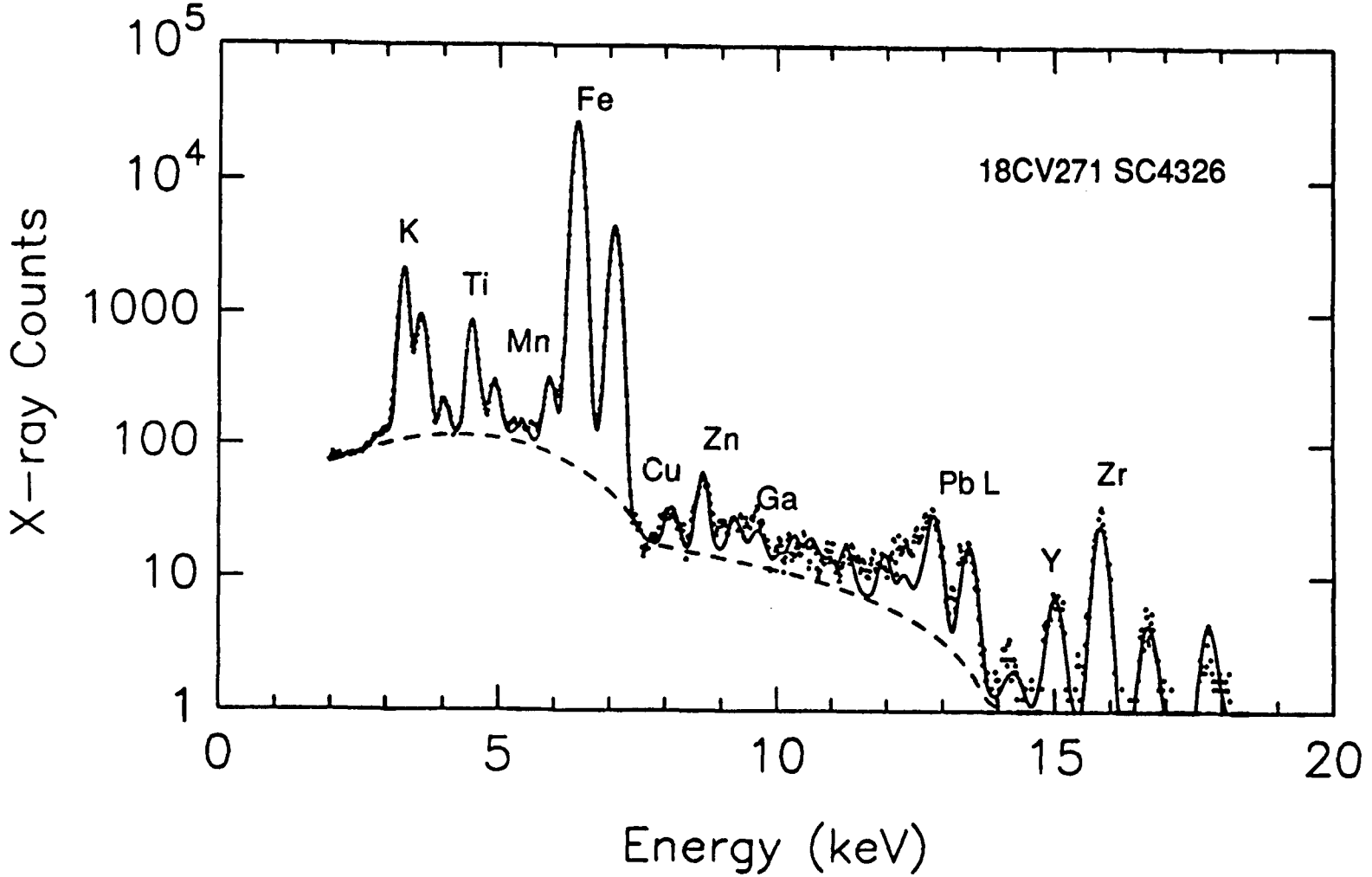

Figure 2. PIXE spectrum for a typical rhyolite projectile point. Points represent the data; the dashed line, a fitted background; and the full line, a fitted spectrum. Characteristic x-ray lines for several elements are labelled.

displayed in a histogram of the number of X rays detected versus the energy of the X ray, as shown in Figure 2.

Accelerated protons striking the target ionize atoms by ejecting an inner-shell electron through a Coulomb interaction. When the vacancy caused by the ejection of the electron is filled by an outer shell electron, as indicated in Figure 3, X rays characteristic of the transition energy are emitted. Each X ray is designated by a Roman letter followed by a Greek letter. The Roman letter indicates the shell in which the initial vacancy is created, and the Greek letter indicates the position in the x-ray series. For instance, Kα indicates a transition from the L shell to the K shell, whereas Lα indicates a transition from the M shell to the L shell. Because the energy levels of each element are different, the X ray emitted is characteristic of the element hit. Detection of these X rays allows determination of the elemental concentration of the target. The energy of the X rays is given accurately by Moseley's Law [12]:

$$(1) \qquad E = Rch\,(Z-1)^2\left(1 - \frac{1}{n^2}\right),$$

where R is the Rydberg constant, c is the speed of light, h is Planck's constant, Z is the atomic number of the emitting atom, and n is an integer (the principal quantum number of the electron shell). Elemental concentrations determined by PIXE are achievable at the part per million level, due to the low background radiation and the high probability that an X ray will be produced by proton irradiation.

The probability of an X ray being emitted through proton irradiation is determined by the x-ray production cross section* of the element. This cross section may be expressed as [13]:

$$(2) \qquad \sigma_x = \sigma\omega k,$$

where σ_x is the x-ray production cross section, σ is the ionization cross section, ω is the fluorescence yield* of the shell concerned and k is the relative intensity of the x-ray

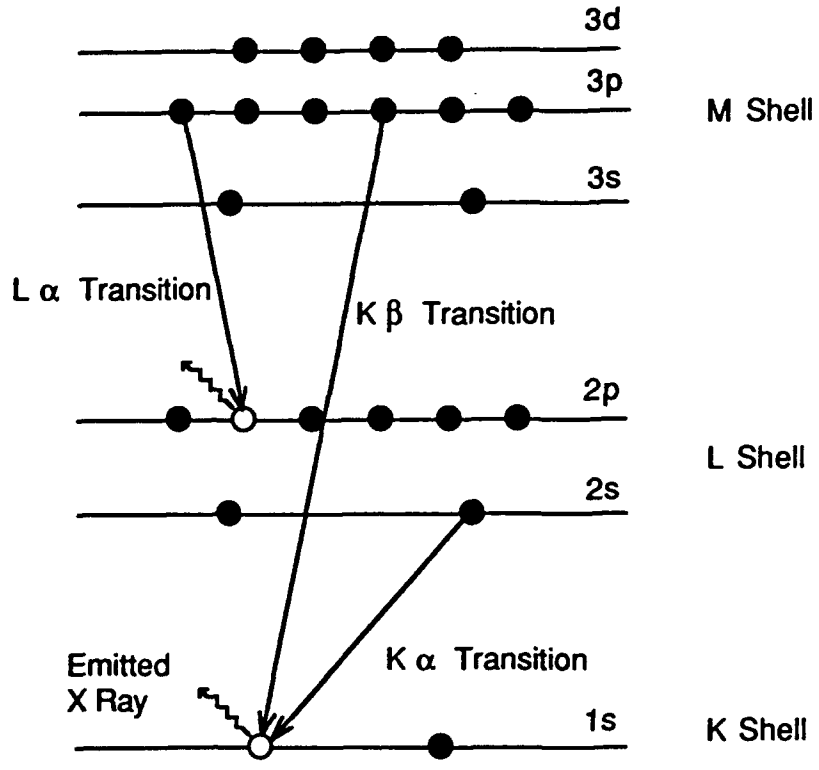

Figure 3. Electron energy levels in a typical atom, showing transitions involved in the emission of various x rays. The spacings of the levels are different for each element, so the energies of the x rays are characteristic of the element.

transition (e.g. Kα, Kβ, Lα, Lβ). Because σ, the ionization cross section, generally decreases sharply with increasing atomic weight, the cross section for heavier elements generally decreases with atomic number. However, x-ray fluorescence increases with increasing atomic number, partially compensating for the decreased ionization cross section, thus allowing detection of the heavier elements [14].

Background* is mostly noticeable in the lower energy portion of the spectrum, where bremsstrahlung* radiation from the incident particles and ejected electrons is prominent. An advantage that PIXE has over electron microscopy in this respect is that the background contribution by proton bremsstrahlung is negligible compared with the sizable contribution made by accelerated electrons in the microscope [15, 16]. Bremsstrahlung from the electrons ejected by proton irradiation is then the major cause of the background in PIXE spectra, and must be accounted for in the analysis of the spectrum [17].

2.2.2. RUTHERFORD BACKSCATTERING SPECTROSCOPY (RBS)

An analytical method best suited for application within a vacuum, Rutherford Backscattering Spectrometry (RBS) has the unique ability among the three IBA techniques considered here to provide concentration information as a function of depth within the sample. RBS, in which incident particles are scattered by target nuclei, has its origins in Rutherford's experiment on the scattering of alpha particles (He^{++}) by gold foils. This method typically uses He^{+} or α particles as the incident ion beam and is concerned with the energy of particles scattered from the target.

The experimental setup for RBS consists of the target, a target positioner, and a charged particle detector located at 160° to the incident beam. Incident particles strike the target and interact through the Coulomb force with the nuclei in the sample. Backscattered particles are detected by the charged particle detector. The energy of the backscattered particle is related to the incident energy by [18]

(3) $$K \equiv \frac{E_{after}}{E_{before}},$$

where the kinematic factor K is simply the ratio of the energy of the incident particle after scattering to the energy of the particle before scattering.

The kinematic factor depends on the masses of the incident and target particles, as well as on the scattering angle [18] :

(4) $$K = \left[\frac{\left(M_2^2 - M_1^2 \sin^2\theta\right)^{1/2} + M_1 \cos\theta}{M_2 + M_1} \right]^2$$

Here, M_1 is the mass of the incident particle, M_2 is the mass of the target particle, and θ is the angle between the paths of the two particles. Thus, heavier nuclei scatter incident ions with more energy than lighter nuclei. For example, in the RBS spectrum shown in Figure 4, the greater energies are indicative of heavier elements, and the "steps" in the spectrum indicate the presence of lighter elements at lower energies.

2.2.3. PARTICLE-INDUCED GAMMA RAY EMISSION (PIGE)

Particle-Induced Gamma-Ray Emission (PIGE) is unlike the first two techniques in that it is a nuclear technique involving short-range nuclear forces, rather than an atomic technique which utilizes the Coloumb force for interaction. As a nuclear technique, it involves overcoming the Coulomb barrier* of the positively charged nucleus and initiating a nuclear reaction in which gamma rays or light particles, or both, are emitted from the nucleus [5]. This can be expressed symbolically as [13]:

(5) $$a + X \rightarrow b + Y + n\gamma,$$

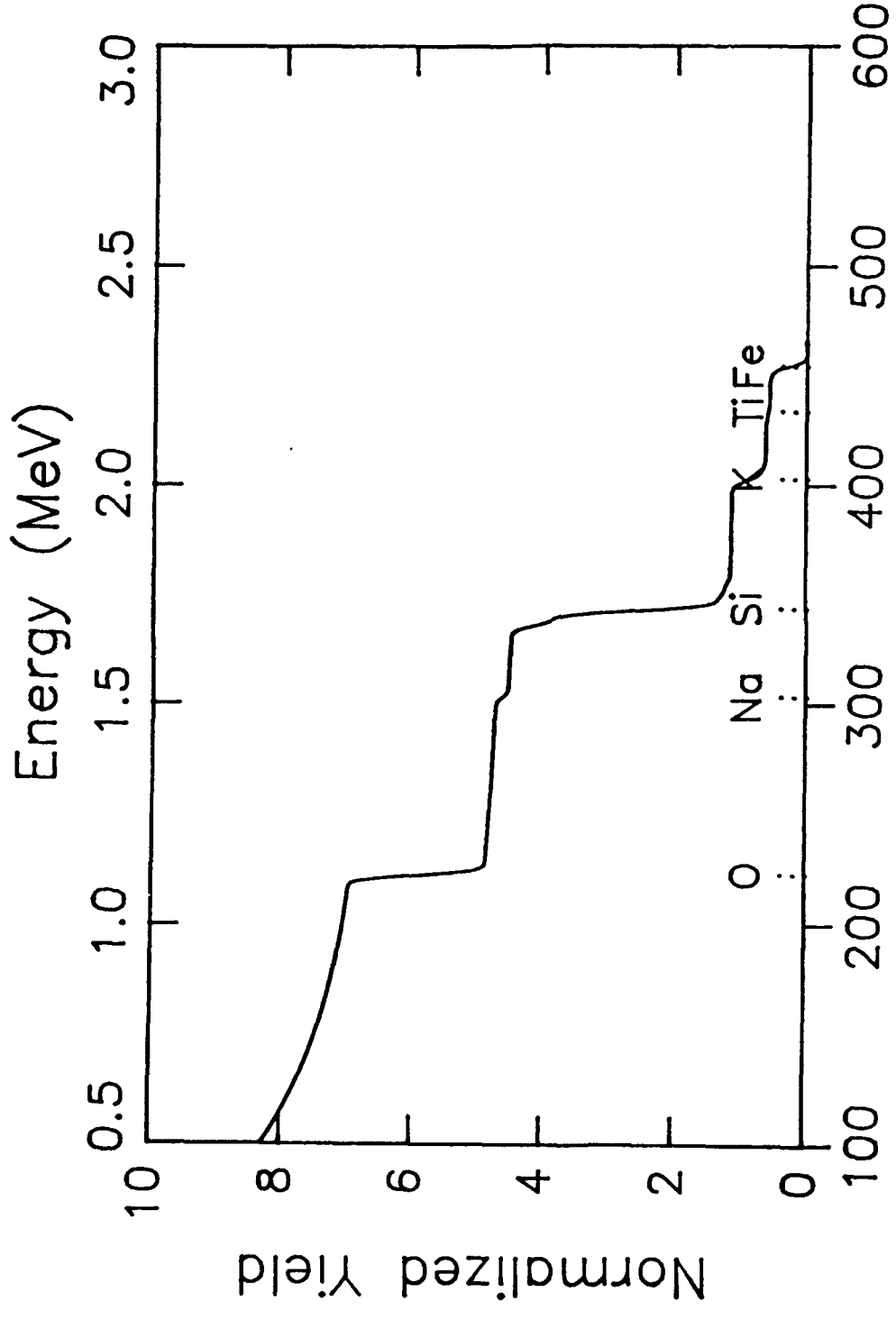

Figure 4. Simulated RBS spectrum for 160-degree scattering of 3-MeV helium ions normally incident on a rhyolite sample of average composition.

where a is the projectile ion, X is the target nucleus, b is a light emitted particle which may be absent, Y is the residual nucleus and nγ represents a number of gamma rays which may be emitted.

The PIGE technique is hampered, however, by the fact that the incident particles often must be above a certain energy in order to overcome the Coulomb barrier and initiate a reaction. Energy conservation requires that [13]:

(6) $$E_a + Q = E_b + E_Y + E\gamma ,$$

where E_a , E_b , E_Y are the energies of the incident particles, emitted particles, and target nucleus, respectively; $E\gamma$ is the total energy released by gamma ray emission; and Q is an energy equal to the change of total rest mass of the nuclei in the reaction. The energy equation (6) is used to determine the incident ion energy necessary to start the reaction. When Q is positive, the reaction is exoergic, and the energy of the incident ions is unimportant, as long as it is sufficient to overcome the Coulomb barrier. If Q is negative, however, the reaction is only possible if the kinetic energy of the incident ion, E_a, can compensate for the energy necessary to balance the equation. An example of such a reaction is:

(7) $$p + {}^{27}Al \rightarrow {}^{28}Si + \gamma,$$

where E_γ = 1.78 MeV and the threshold proton energy is 991.91 keV. This reaction was used to energy calibrate the analyzing magnet, and will be discussed in section 3.4.

2.4. SELECTION OF IN-AIR PIXE

A literature search provided information about experimental setups, analysis methods, software availability, and applications of the IBA techniques discussed. An overwhelming amount of support for the use of PIXE in trace elemental studies was found across the board. PIXE, which dates back to 1970 [19], is a maturing method and the

recent availability of reasonably priced accelerator systems in the 1-3 MeV range has boosted its popularity for bulk analysis, and of RBS for depth profiling.

The use of protons as the bombarding particle is the first distinction which sets PIXE apart from RBS. Alpha particles, usually used in RBS, only penetrate the sample on the order of 10 microns, providing a limited depth profile. On the other hand, a bulk view is provided by protons, which penetrate tens of microns into the sample because they have smaller mass and less charge [19]. PIXE is also well suited to use in air. In air, alpha particles are quickly absorbed, hindering detection of the backscattered ions when conducting experiments outside the accelerator vacuum . Additionally, the surface barrier detectors which are used in the detection of charged particles are extremely sensitive to light, and would require rather special attention if used outside of the vacuum chamber.

Perhaps an even greater advantage of PIXE is the ease of analysis of a spectrum from a sample. In this respect, the PIGE method is far behind both PIXE and RBS, as there is no widely-used computer analysis code available to study gamma-ray spectra, whereas widely-accepted analytical codes for PIXE and RBS are available commercially. PIXE also has the advantage that rough analyses may be performed while the target is still being irradiated, because an x-ray spectrum is composed of peaks of X rays of known energies, forming a "handprint" of the elements present which is easily read and understood even before rigorous analysis.

Simplicity of sample preparation and positioning were also factors in the selection of the PIXE method. The facilities for in-vacuo studies at NATALY are still in the development stage, and are limited by the equipment available at present. At this time the target positioner in the scattering chamber is only 10 cm in length, allowing it to hold 2-3 small projectile points at a time, and is limited to linear movement in and out of the beam. Contemporary facilities using PIXE for in-vacuo analysis have boasted computerized servo motors for precise positioning of the sample [20], or meter-long sample holders capable of

suspending many targets in the vacuum at one time [21], which allow the flexibility to precisely position targets and change samples without breaking vacuum. In order to achieve that same flexibility of movement and rapidity of sample analysis, the experiments reported in this work were performed outside the vacuum of the beamline in a target box designed specifically for in-air PIXE.

In addition to the ease of positioning and the changing of samples which accompanies in-air analysis, other advantages were also identified. Charging of the sample in vacuum, for example, a difficulty which could lead to the object being charged to several kV, was completely avoided. Although some groups have reported success in overcoming this difficulty by directing a stream of electrons across the sample being analyzed, placing the sample in air solved the problem simply, as ionized atoms soon recaptured electrons and regained electrical neutrality [13]. A problem which accompanies charging of the sample, heating, was similarly avoided; the atmosphere acted as a heat sink and removed the excess thermal energy.

3. EXPERIMENTAL ARRANGEMENTS

3.1. GENERAL

Analysis of the stone tools was accomplished using a system based upon an NEC Pelletron 5SDH Tandem Electrostatic Accelerator shown in Figure 5. This accelerator can produce proton beams of energies from 100 keV to 3.4 MeV or helium beams with energies from 100 keV to 5.1 MeV [23].

3.2. ION SOURCE

An NEC Alphatross source was used to create negative ions and inject the particles into the accelerator. In the case of a proton beam, an H^+ plasma is created in the source bottle when hydrogen gas is ionized by RF radiation. A probe voltage of 5-6 keV pushes the negative ions into a charge exchange chamber where 1-2% of the ions interact [23] with rubidium gas according to [24]:

(8) $$He^{+} + Rb \rightarrow He^{0*} + Rb^{+}$$

and:

(9) $$He^{0*} + Rb \rightarrow He^{-} + Rb^{+}$$

forming H^- ions which then enter the low energy end of the accelerator. In equations (8) and (9), H^{0*} refers to a neutral helium atom in an excited state.

3.3. ACCELERATOR

As shown in Figure 6, a positive terminal at the center of the accelerator attracts the negative ions from the source, accelerating them to the potential, V, of the terminal. Passage through a volume containing low-pressure N_2 "stripper" gas converts the incident negative ions into positive ions by removing electrons [25]. The positive ions thus created are accelerated away from the positive terminal toward the high energy end of the

Figure 5. (Next page) Overview of the Naval Academy Tandem Accelerator Laboratory (NATALY), showing the accelerator and the control console. The ion source is toward the far side of the room, and the focusing and momentum-analyzing magnets are toward the near side, on the left hand side of the photograph.

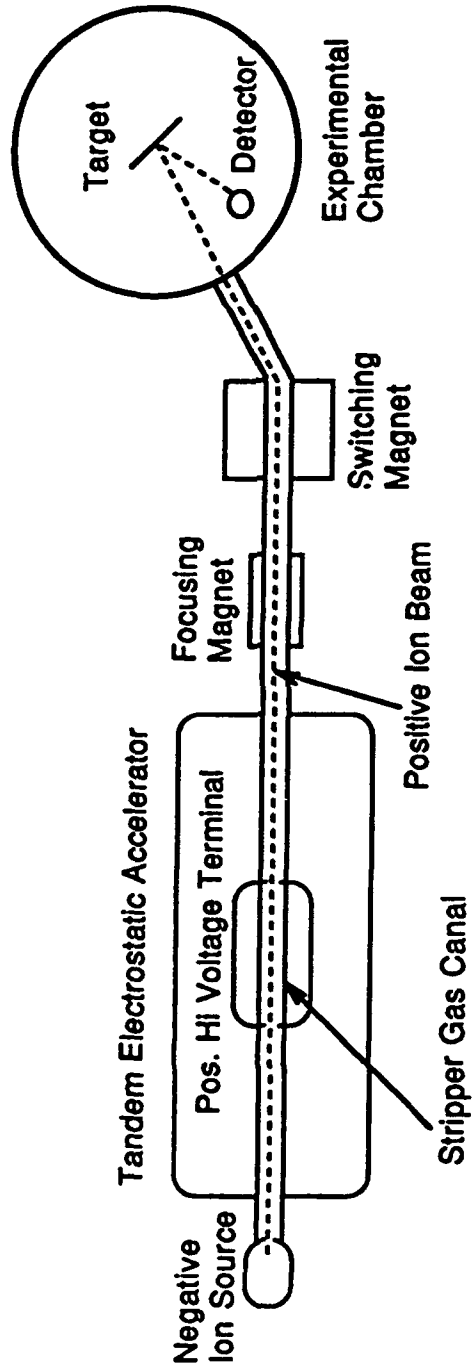

Figure 6. Schematic of the tandem electrostatic accelerator system.

accelerator, increasing the energy of the particle by a factor of two or more. In general, particles with a charge state of +n attain a final energy of (n+1) eV, where e is the electronic charge. A terminal voltage of V = 1.3 MV was therefore the terminal potential necessary to create the 2.6 MeV protons used to probe the rhyolite tools.

3.4. BEAMLINE

After leaving the high energy end of the accelerator the protons are focused into a beam by a magnetic quadrupole lens, then deflected by an analyzing magnet into the beamline, shown in Figure 7. The analyzing magnet is also used to determine the energy of the beam particles using the relation

$$(10) \quad B = K \frac{\sqrt{EM}}{q},$$

where B is the magnitude of the magnetic field in gauss, K is a calibration constant that depends on the angle the beamline makes with the accelerator, E is the energy of the particle in MeV, M is the mass of the particle in MeV, and q is the charge of the ion expressed in multiples of the charge on the electron .

The calibration constant K for the beamline was measured using the $^{27}Al(p,\gamma)^{28}Si$ reaction, which produces a surplus of gamma rays (a "resonance") when the proton energy is precisely 991.91 keV. The resonance was experimentally observed to occur with a magnetic field of B = 2155.5 gauss, yielding a value of K = 70.636 e gauss/ MeV, according to equation (10).

After the analyzing magnet deflects the beam into the beamline, the shape of the beam is measured with a beam profile monitor, and the beam current can be measured and optimized by inserting a Faraday cup into the beam path. Stabilization of the beam at the selected energy, E, is accomplished by a feedback system that monitors the current striking

Figure 7. (Next page) The milliprobe beamline. The components are explained in the caption for Figure 8.

a pair of slits after the analyzing magnet in the beamline, indicated in Figure 8. After the energy control slits, the beam passes into the scattering chamber. At this point, the beam may be used for backscattering experiments in the scattering chamber, or it may be allowed to pass through the chamber to the quadrupole electrostatic lens.

3.5. TARGET AREA

After final focusing with the electrostatic lens, the beam passes through a thin Kapton window into the atmosphere within the target box. Samples for PIXE or PIGE studies may be analyzed outside of the 10^{-6} torr vacuum of the beamline.

The target enclosure shown in Figures 9 and 10 was designed to accommodate the ion beam, the sample, and the x-ray detector in a specific geometry. The detector used in this work was a lithium-drifted silicon detector, or Si(Li) (pronounced "silly") detector. A detector angle of 125° to the beam propagation direction was achieved by mounting the Si(Li) detector on a separate platform next to the target box. More commonly used geometries place the Si(Li) detector at 90° or 135° from the incident beam. A detector angle of 135° is preferred, when possible, due to the more than 50% reduction in bremsstrahlung background radiation at this angle compared with a 90° angle, giving a cleaner spectrum [19].

Samples were mounted on an aluminum sample holder which was positioned perpendicular to the Si(Li) detector and maintained a sample to detector distance of 18.5 mm. The aluminum target stand was electrically isolated from the target box through the use of teflon screws, in order that any protons incident on the aluminum holder would provide a more consistent measure of current and total charge.

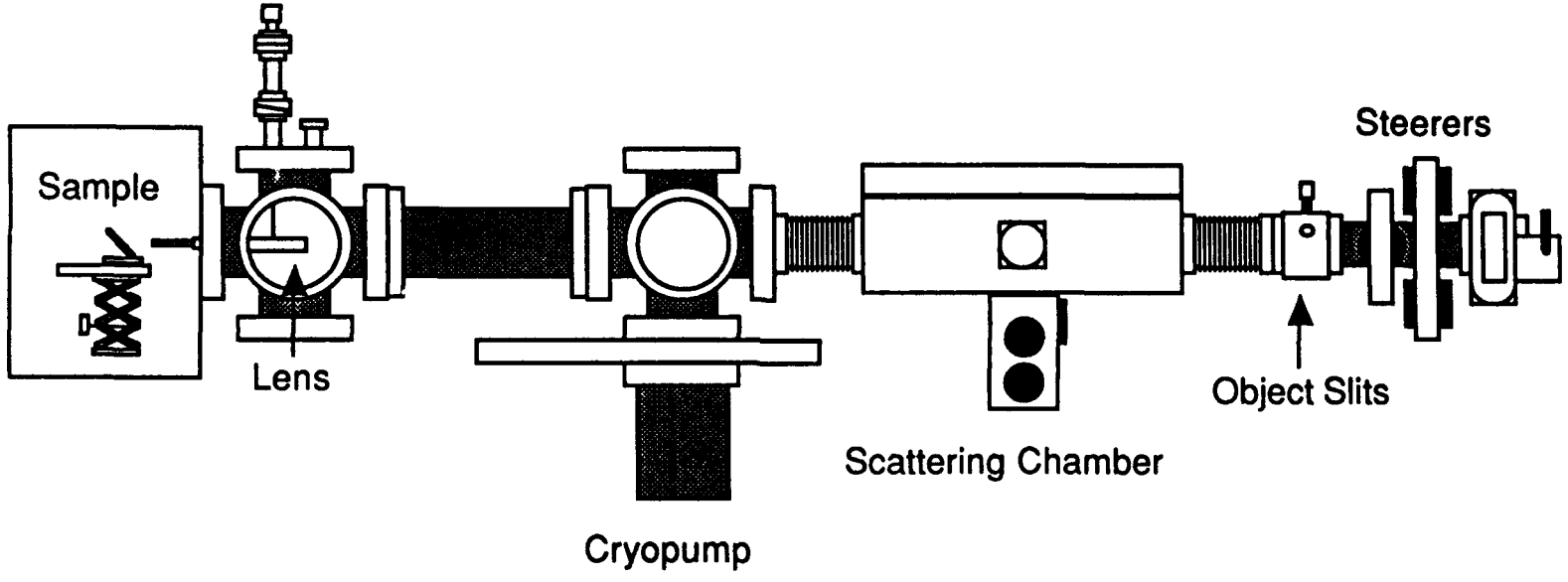

Figure 8. Milliprobe beamline. The ion beam travels from right to left, entering the atmosphere and striking the sample in the enclosure at the left end. The size of the beam spot on the sample is approximately 1 mm. The Si(Li) detector is hidden in this view by the lens housing.

Figure 9. (Next page) Close-up view of the sample chamber. A rhyolite projectile point is in the holder at the center of the view, and the x-ray detector is on the left. The components are explained in more detail in the caption for Figure 10.

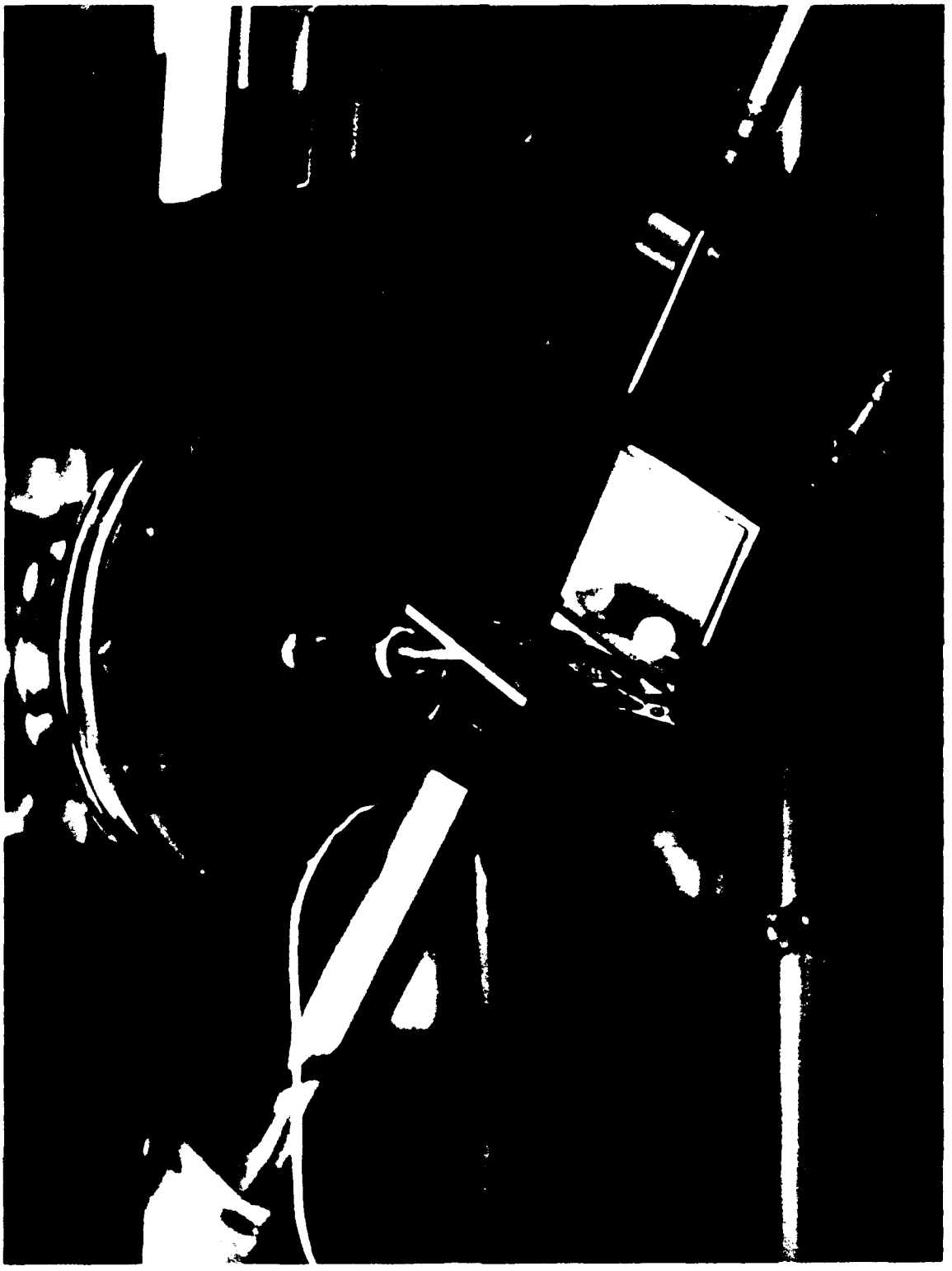

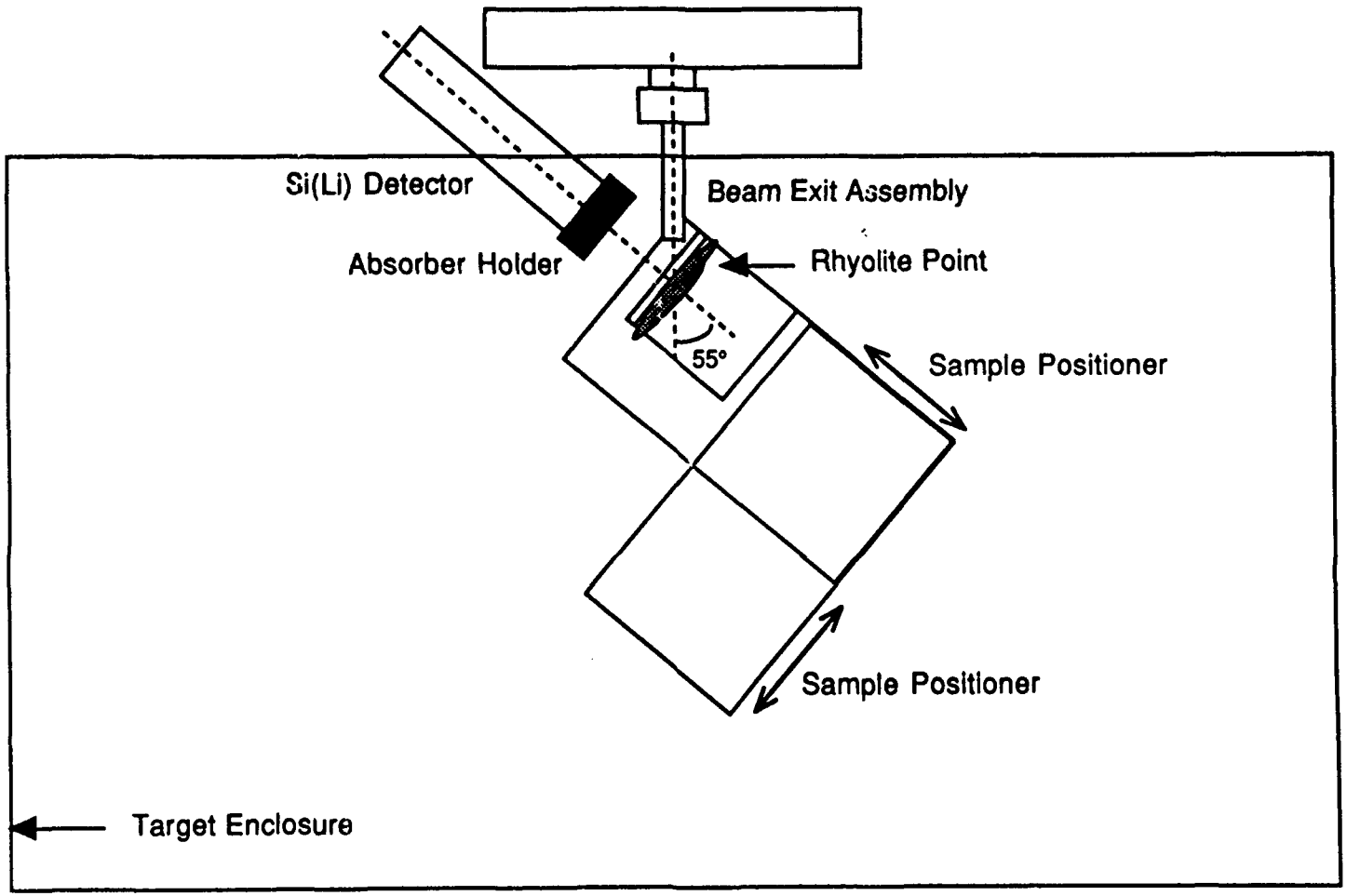

Figure 10. Top view of the sample chamber. The ion beam enters the chamber through the "Beam Exit Assembly" at the top of this view, and strikes the rhyolite point. X-rays emitted at an angle of 125 degrees from the beam direction enter the Si(Li) detector after passing through an interchangeable absorber.

3.6. X-RAY DETECTOR

A Si(Li) detector was preferred over available germanium FET detectors (Ge detectors) due to the better resolution for low energy X rays achievable with Si(Li) detectors [26], and because of the availability of a computer code which was designed to account for the performance of a Si(Li) detector in the analysis of x-ray spectra [9]. Resolution of the detector used in the analysis of the projectile points, based on the FWHM* of the Cr Kα X ray, was typically between 205-215 eV. The efficiency of the detector was determined by the inherent operation of the Si(Li) detector and by the addition of filters positioned between the sample and the detector using the equation [17]:

(11) $$\varepsilon = T\,\varepsilon_i\, f_g\, f_{Be}\, f_{Au}\, f_d\, f_R,$$

where ε is the total detector efficiency coefficient, T is the energy-dependent transmission coefficient for optional filters, ε_i is the intrinsic efficiency, f_g is a geometric factor dependent on photon energy, f_{Be}, f_{Au} and f_d are transmission coefficients for the beryllium detector window, gold layer and silicon dead layer, and f_R is the correction for radial dependence.

Operation of the Si(Li) detector is based upon electron-hole pair production* within the silicon diode in the detector [26]. X rays emitted by the target enter the detector through a 0.0254 mm beryllium window and pass through a 200 Å thick gold contact layer before entering the silicon diode itself which is maintained at a cryogenic temperature to reduce electronic noise. The first 0.1 mm layer of the silicon semiconductor is called a "dead" layer, because this layer collects no charge and acts only as an absorber [26,27]. The active part of the detector, a 10 mm radius, 5.30 mm thick lithium-drifted silicon crystal, is the final part of the diode, and this is where charge is collected from the absorption of the X ray. The pairs produced by the X ray are formed here and attracted to opposite electrical contacts by a bias of 1000 V across the diode, which induces a current pulse in the preamplifier. Integration of the current pulse in the preamplifier produces an output voltage

with a height proportional to the incident x-ray energy. As shown in Figure 11, the output voltage is then amplified by an Ortec 572 spectroscopy amplifier and analyzed by an MCA* card in a Zenith-248 computer, described in section 3.8. After a spectrum has been acquired, it is shipped to a micro-VAX computer for analysis.

3.7. X-RAY FILTERS

Filtering of X rays incident on the Si(Li) detector using absorber materials was necessary to eliminate pile-up of X rays from the major constituents of the rhyolite elemental matrix. Pile-up, a common problem in PIXE studies, occurs when two X rays enter the detector at the same time. The detector puts out a pulse of height corresponding to the sum of the energies of the two X rays. Using a filter designed to selectively absorb X rays produced by major constituents reduces the photon flux incident on the detector to a point where the probability of two X rays entering the detector within the detector's resolving time is small [1-4, 19-22]. Previous studies of rhyolites indicated that the major constituents of these rocks are Si, Al, Fe, Na, and K, which generally compose 98% of a rock by weight [8]. These studies, it should be pointed out, employed wet-chemical (destructive!) techniques.

Because rhyolites had not been previously studied using IBA techniques, it was necessary to select a filter which would maximize detection of trace elements through the attenuation of X rays produced by the major constituents of metarhyolite. Studies of obsidian, a metamorphic rock of composition similar to that of metarhyolite, have been carried out at the Lucas Heights Research Laboratories in Australia using a "funny" filter, a filter made of Perspex or graphite with a small hole laser drilled through the center [17, 28]. This filter had little effect on the high-Z trace elements of interest, but stopped most of the X rays from elements Si, K, Ca or lower, some of which were still observed with low efficiency because of the hole in the filter [28]. Studies of other silicon-matrix artifacts,

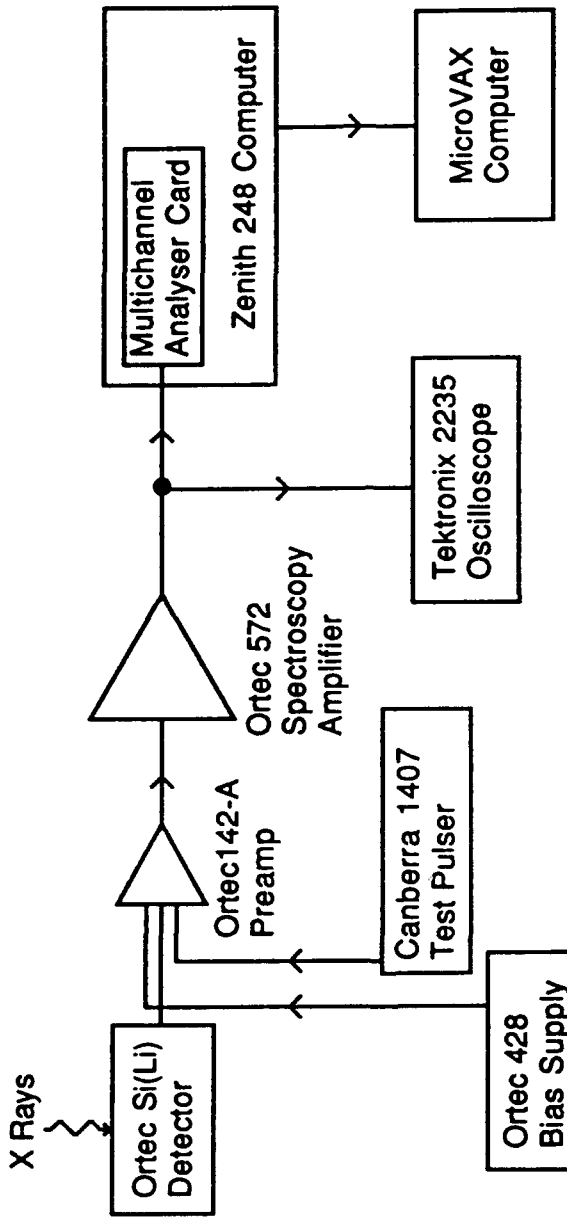

Figure 11. Block diagram showing the equipment used for data acquisition and analysis.

such as ancient glasses, have been carried out at the Bartol Research Institute using filters which combined aluminum, vanadium and mica in order to attenuate X rays from elements as heavy as iron [29].

This study utilized an aluminum foil of 0.025 mm thickness as an absorber in order to eliminate Si x-ray pile-up and attenuate the potassium x-rays. A filter transmission coefficient,

(12) $T = \exp[- (118.338) \cdot (E^{-2.8317})]$,

where E is the photon energy in keV, and the 118.338 is an empirical constant, was developed for the computer model using cross section data compiled by Veigele [30]. Iron, however, remained a dominant feature in the spectra, and an attempt to implement a filter of 0.025 mm Al and 0.025 mm V in order to attenuate the Fe X rays was postponed due to difficulty in developing a proper transmission coefficient that could model the attenuated iron X rays properly.

3.8. DATA ACQUISITION SYSTEM

An analog-to-digital converter in the MCA package converted the voltage pulses provided by the Si(Li) detector into numbers proportional to the height of the pulse, called "channels". The program then counted the number of pulses received in a given channel and created a histogram of the data such as shown in Figure 12. This histogram is the raw data of the PIXE spectrum, and can be used to determine what major elements are present in a sample through visual inspection of the computer display. An ASCII output of each spectrum was then reformatted using FIXPIX [31], in order for the data to be in the correct form for input into PIXAN [17], a PIXE analysis program package. Typically 10 spectra are grouped into one formatted data file so that "batch jobs" can be analyzed by BATTY, a program in the PIXAN package.

Figure 12. (Next page) A view of the Nucleus PCA-II computer screen, showing a PIXE spectrum of a rhyolite projectile point. The green vertical lines mark the positions of the X rays emitted by Ca atoms in the sample.

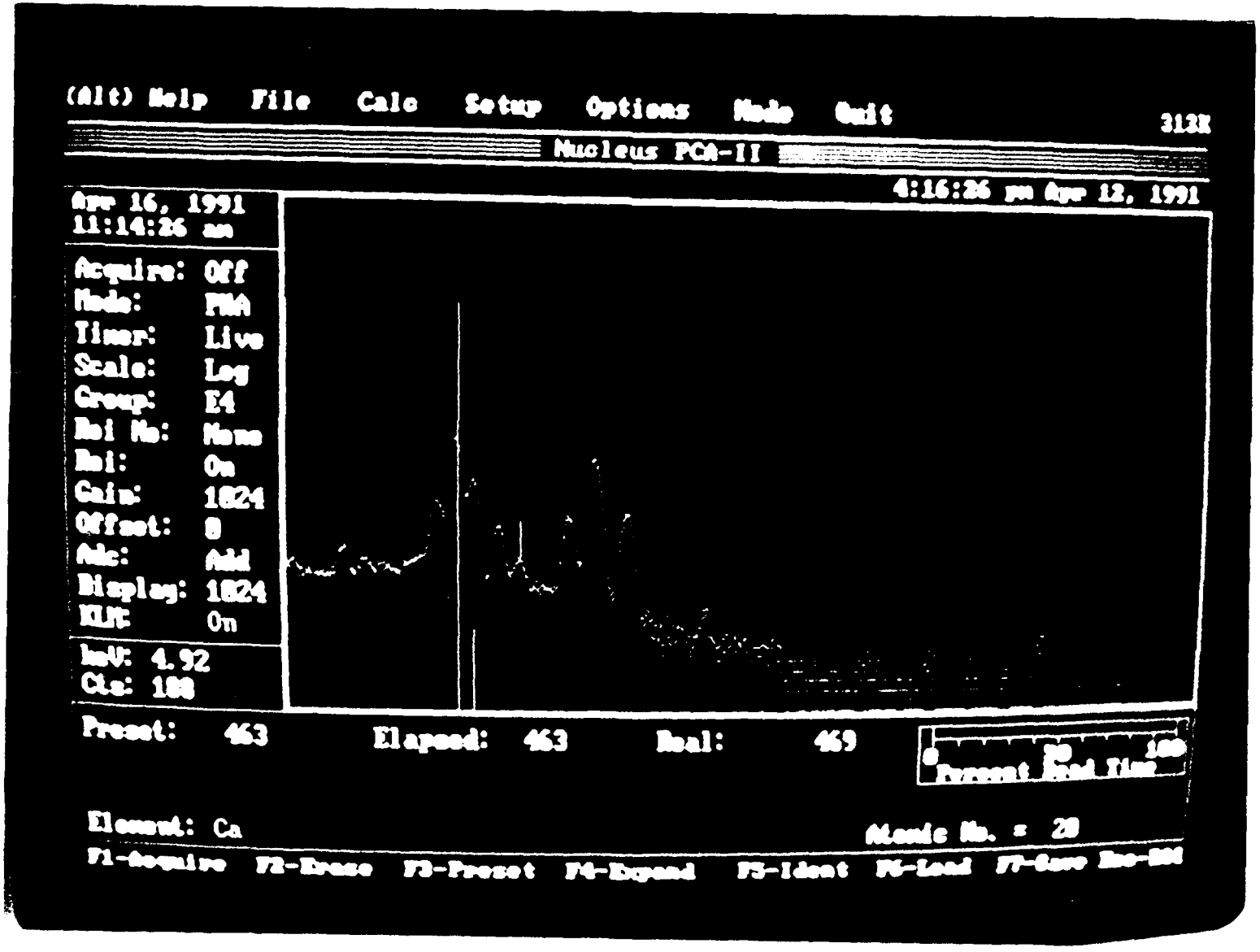
(Alt) Help File Calc Setup Options Mode Quit
Nucleus PCA-II
Apr 16, 1991
11:14:26 am
4:16:26 pm Apr 12, 1991
Acquire: Off
Mode: PHA
Timer: Live
Scale: Log
Group: E4
Mul No: None
Mul: On
Gain: 1024
Offset: 0
Adc: Add
Display: 1024
XLT: On
Preset: 463
Elapsed: 463
Real: 469
Element: Ca
Movie No. = 20
F1-Acquire F2-Erase F3-Preset F4-Expand F5-Ident F6-Load

3.9. MEASUREMENTS

In-air PIXE was used to analyze 51 of the projectile points provided by the Maryland Historical Trust. No special preparation of the samples other than the initial washing and brushing was found necessary.

The beam energy was calibrated to provide a 2.5 MeV beam on the target, because the ionization cross section and x-ray branching ratios used in the data analysis program were calibrated for that energy. Passing through the 7.5 μm Kapton window at the end of the beamline and 10 mm of air between the window and the target , however, protons lose 0.167 MeV, thus the accelerator and beamline were calibrated for a beam energy of 2.667 MeV. To achieve a beam energy of 2.667 MeV before extraction into the air required a terminal potential of approximately 1.35 MV, and a field of 3534.5 gauss in the analyzing magnet.

With this experimental setup, and a beam current on target of approximately 200 pA, it required approximately 15 minutes per spectrum to achieve an integrated charge of 0.1 μC on target. An electrical lead attached to the aluminum target stand was used to monitor the beam current and total charge received by the target.

Two kinds of tests were conducted to investigate possible systematic errors in the measurement procedures. Elemental concentrations deduced from the spectra depend on an accurate knowledge of the total integrated charge on each sample. Several spectra obtained with the ion beam on the same sample spot produced yields of Fe that agreed within 0.5%, K and Pb yields that were consistent within 2%, and Ca, Ti, and Mn yields that agreed within 5%.

Because of the presence of possible spatial nonuniformities in the samples, tests were conducted to investigate the effects of analyzing different sample areas. Repeated measurements at different spots on two samples were carried out by displacing the sample in steps of 1 mm. Analysis of the spectra obtained indicated concentration differences of

less than 10% for Mn and Pb; 10 to 20% for Fe, K, and Ti; and 30 to 40% for Ca . These variations could be minimized in future experiments by implementing a motorized sample positioner that would move the sample during analysis and average the measured composition over a larger area.

4. DATA

4.1. PIXE SPECTRA

Spectra like the one shown in Figure 12 were acquired for the 51 targets. Settings on the Ortec 572 spectroscopy amplifier were: Coarse Gain = 200, Fine Gain = 9.49, and Shaping Time Constant = 6 μsec. The unipolar output pulses were used. Each spectrum required approximately 15 minutes to acquire.

4.2. DATA ANALYSIS

Spectrum analysis required the use of four different computer programs: the Nucleus Multichannel Analyzer (MCA), FIXPIX, BATTY, and THICK. The MCA program converts the analog data from the Si(Li) detector to digital data and sorts them into a spectrum. FIXPIX is used to reformat the output from the MCA program so that it may be read by BATTY. BATTY, part of the PIXAN analysis package, determines the yield of each element present in the spectrum, while THICK, another part of that package, provides coefficients used to determine the absolute concentrations of trace elements in the target from the elemental yields.

The MCA program was run on a dedicated Zenith Z-248 computer located next to the beamline. BATTY and THICK were also initially run on Zenith Z-248 computers, but long analysis times (several hours to analyze the data taken in one day), made this inconvenient. Acquisition of a Micro-VAX computer at NATALY and the subsequent implementation of PIXAN on this computer reduced analysis time considerably (approximately five minutes for a day's worth of data).

4.2.1. DETERMINATION OF ELEMENTAL YIELDS: PROGRAM BATTY

This part of the PIXAN package analyzes each spectrum, computes and subtracts the background contribution, and determines the area under each x-ray peak. Modeling an

x-ray spectrum as modified Gaussian peaks on a background, BATTY uses a non-linear least squares fitting procedure to determine the peak areas of the spectrum [17]. The spectrum model at channel i having x-ray energy E_i is expressed as:

(13) $$Y(E_i) = Back(E_i) + PN + \sum A_j R_{jk} G_{jk}(E_i)$$

where $Back(E_i)$ is the background, PN is a parameter used to fit the high energy end of the background, A_j is the height of an arbitrary reference x-ray peak for element j, R_{jk} is a matrix of the relative intensities of all the characteristic peaks of element j, G_{jk} is a characteristic peak shape function based on a modified Gaussian peak, and the summation is over all elements (j) and for all peaks (k) for an element j. Because proper fitting of the rhyolite spectra necessitated tweaking the type of background fit and the function R_{jk}, which determines the relative line intensities, both of these variables will be discussed in more depth.

Background radiation in the region from 1 to 10 keV is assumed to be secondary electron* bremsstrahlung and can be modeled using either a polynomial fitting procedure or an iterative "peak filling" function. Initial attempts to use the polynomial background fitting procedure to fit the background of the rhyolites studied induced the program to crash, and were discontinued in favor of the iterative background. The peak filling function first selects every second point below 10 keV and every fifth point above that energy and approximates the background. An iterative procedure then removes peaks using the test:

(14) $$Y_i > 0.5\,(Y_{i-1} + Y_{i+1}) = m_i\,,$$

that is, if the height, Y_i, is greater than the mean of the two adjacent points it is replaced by the mean and the process continues [17].

The relative intensities of the characteristic x-ray lines emitted from an element are dependent on the incident particle and, in the case of L X rays, the energy of the particle [17]. The detector, however, does not necessarily find the same ratio because of

absorption in the sample itself, in the air, in the detector equipment, and in the filter used. The corrected relative intensity expression:

(15) $R^{c}_{jk} = R_{jk}\,\varepsilon(E_{jk})\,C$,

where $\varepsilon(E_{jk})$ is the efficiency of the detector given in equation (11) and the self-absorption correction C is for the 125° backward angle of the detector, takes into account any absorption due to those factors.

The program then fits the spectrum using the calculated background and the fitted characteristic peaks. Output of the program appears as shown in Figure 13, where three different spectra are illustrated. Differences in the elements present and the yield of those elements produces a different background curve for each spectrum.

BATTY then determines the areas of the characteristic peaks through a procedure which minimizes the difference between the raw data and the model spectrum. The total yield of an element is then found by multiplying the area of the reference peak with the relative line intensity coefficients and summing those products with the area under the characteristic line peak. This total yield for each element can then be converted to an absolute concentration using a coefficient calculated in the THICK program.

4.2.2. DETERMINATION OF ABSOLUTE CONCENTRATIONS: PROGRAM THICK

THICK is used to determine the expected yield per unit concentration of an element so that the absolute concentration may be calculated from the yield determined by BATTY. Calculation of the yield per unit concentration requires consideration of the effects of a thick target on x-ray production and absorption, accumulated charge on the sample, the detector solid angle and the detector efficiency. The coefficient value determined, M, can be used to determine the absolute concentration through the simple equation [17]:

(17) Yield = (Concentration) x (M).

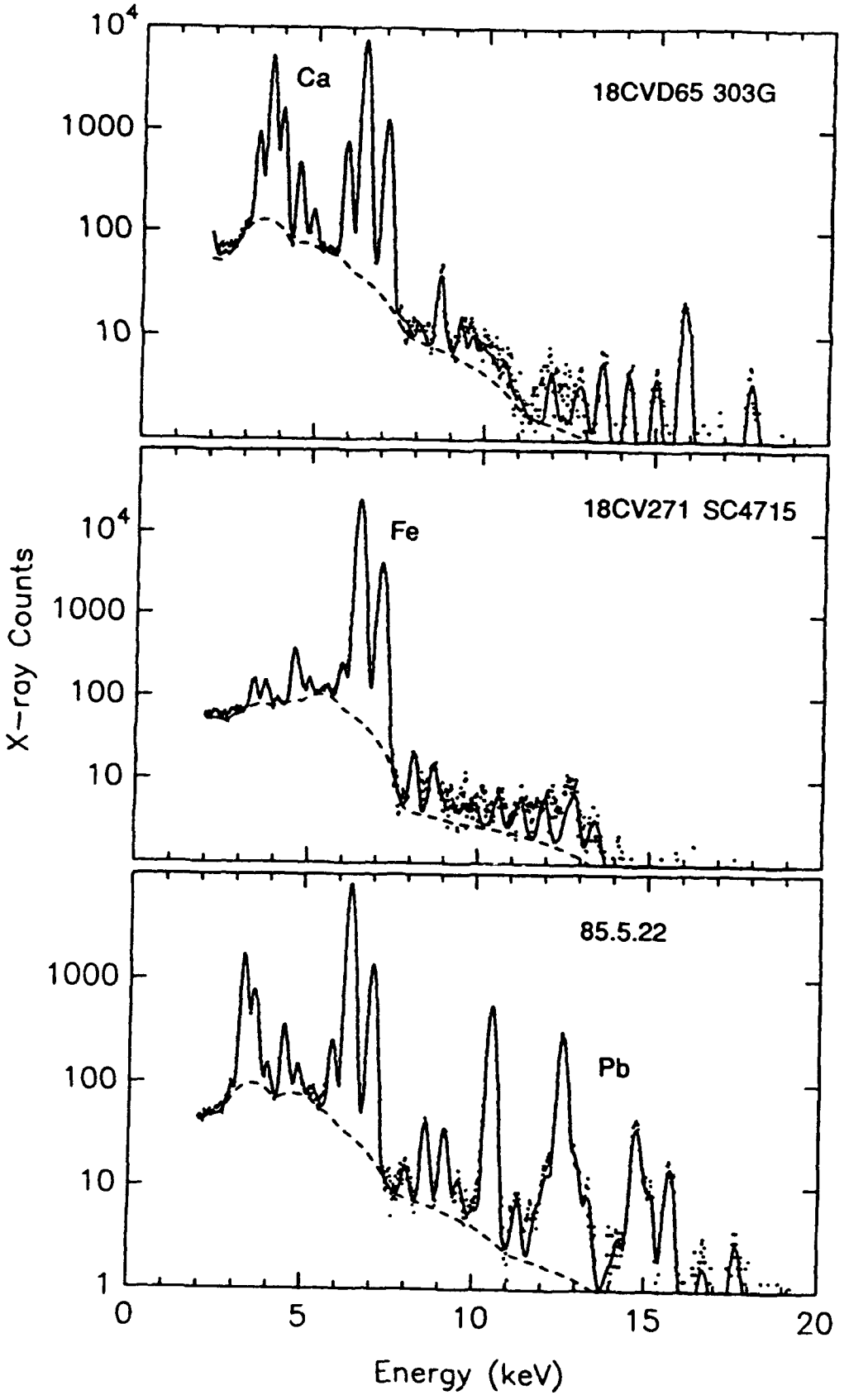

Figure 13. PIXE spectra for three rhyolite projectile points. Differences in composition are apparent.

Concentrations of trace elements detected in the 51 stone tools analyzed are displayed in tables II and III. The 10 trace elements listed in table II were found consistently in the samples studied. Table III lists the concentrations of other elements found less often in those samples, but which may be used to further determine similarities or differences in the clusters formed through statistical analysis.

Table II. Concentrations (parts per million, by weight) of ten elements detected in most of the rhyolite projectile points. The entry "nd" indicates that an element was not detected in a particular sample. Statistical uncertainties due to background subtraction and peak fitting are less than 1% for Fe and K; less than 10% for Ca, Ti, Mn, Zn, and Zr; and 10-30% for Cu, Ga, and Rb.

SEQ. NO.	Fe	K	Ca	Ti	Mn	Cu	Zn	Ga	Rb	Zr
1	17595	56944	2815	1646	367	38	175	39	171	453
2	11441	19853	1194	564	185	20	58	28	106	677
3	14043	27100	7177	1085	323	21	79	27	55	554
4	9263	47150	755	468	158	8	54	22	156	533
5	15885	32432	803	666	207	11	42	31	104	731
6	9804	22181	2299	900	188	18	49	30	46	626
8	18734	24605	4733	1206	473	18	53	37	45	586
9	14609	10370	723	628	106	9	57	38	37	112
10	9802	32172	184	399	170	6	29	17	104	284
11	16403	40251	2594	1113	296	24	95	49	120	348
12	41978	39922	1755	1640	286	44	142	66	29	1038
13	15765	32853	307	602	96	22	98	38	33	289
14	43487	1867	361	616	261	47	41	9	nd	nd
15	10286	35082	850	653	191	7	51	37	93	622
16	12165	30158	667	462	142	nd	18	11	88	505
17	11264	34159	1609	951	543	4	174	33	103	535
18	15609	24020	558	606	157	14	46	34	45	174
19	15791	20656	1913	586	308	20	53	43	19	1569
20	10489	42326	1647	938	437	22	147	32	110	599
21	20080	32033	580	632	183	nd	53	33	86	371
22	11978	48312	1071	961	148	23	40	21	123	266
23	17095	22872	1049	804	109	15	48	34	53	771
24	10574	29337	659	586	212	11	25	33	86	643
25	11561	16906	33100	875	1091	12	93	31	67	798
27	16556	28121	4154	890	442	10	65	32	68	750
29	15192	33227	2350	977	305	13	628	34	87	605
30	13960	41800	1437	1230	247	2	32	20	115	255
31	20301	23540	1736	771	475	4	25	41	60	853
32	13261	24974	1081	1237	321	4	62	39	52	673
33	41941	51812	3558	1812	705	44	111	48	92	894
34	24518	26236	480	572	235	14	51	11	38	681
35	11902	52994	3362	964	694	26	66	44	149	975
36	13744	38551	1050	718	338	11	112	26	124	717
37	17031	36180	1253	5035	400	18	118	27	162	668
38	18763	46556	1478	1298	660	5	39	31	117	849
39	15138	35572	554	617	182	11	117	42	93	764
40	9737	48473	1759	716	139	18	40	35	123	937
41	13288	40344	692	506	261	15	76	23	102	312
42	11862	35337	1198	1290	350	14	132	24	131	405
43	13162	35103	1709	606	353	25	56	22	48	589
44	14830	31499	1285	500	133	25	52	27	108	689
45	8200	35302	2008	1304	319	9	99	21	110	389
46	12353	45070	759	492	120	40	68	17	140	449
48	11540	33530	1191	629	226	33	79	23	143	629
49	18554	28641	1091	521	371	32	75	36	99	787
50	13567	35592	1755	648	340	22	119	34	54	638
51	11889	22267	1943	597	109	108	64	22	47	620
52	36488	5964	2096	227	251	13	26	13	nd	168
53	9659	38064	1370	286	130	27	95	21	137	373
54	20201	45386	1235	1492	194	14	43	33	64	1013
55	23038	55079	835	731	332	34	88	27	78	1040

Table III. Concentrations (parts per million, by weight) of nine additional elements detected in a smaller number of points. The entry "nd" indicates that an element was not detected in a particular sample. Statistical uncertainties due to background subtraction and peak fitting are larger than in Table II; concentration values smaller than 50 parts per million may not be significant.

SEQ. NO.	Cr	Ni	Se	Br	Sr	Y	Nb	BaL	PbL
1	nd	nd	nd	nd	43	90	129	628	114
2	4	nd	nd	nd	nd	84	nd	37	nd
3	10	nd	nd	nd	nd	92	60	nd	nd
4	8	2	nd	9	nd	nd	nd	nd	nd
5	13	nd	nd	19	nd	78	70	nd	nd
6	6	nd	nd	nd	34	83	94	27	nd
8	12	nd	16	29	56	69	97	72	60
9	10	nd	21	28	nd	nd	nd	32	68
10	nd	nd	nd	nd	nd	nd	nd	430	nd
11	nd	nd	19	30	36	132	97	542	129
12	10	nd	84	104	nd	196	192	nd	239
13	1	nd	nd	10	nd	27	nd	400	68
14	41	2	36	55	nd	nd	nd	nd	85
15	1	2	nd	nd	nd	39	nd	nd	nd
16	6	nd	nd	nd	nd	27	nd	nd	nd
17	6	nd	nd	nd	nd	36	68	nd	nd
18	3	nd	19	28	nd	nd	nd	496	nd
19	20	nd	22	34	50	212	nd	261	143
20	5	3	nd	nd	nd	94	nd	22	nd
21	11	nd	nd	11	nd	290	nd	nd	nd
22	5	nd	9	9	nd	32	nd	436	nd
23	12	3	25	28	nd	63	49	nd	nd
24	3	2	nd	nd	nd	28	52	108	nd
25	10	3	nd	34	89	93	nd	nd	46
27	11	nd	14	15	38	57	69	nd	nd
29	16	nd	13	18	nd	84	42	40	69
30	nd	3	nd	nd	29	144	60	353	nd
31	6	nd	nd	nd	29	56	99	98	72
32	4	nd	nd	11	nd	66	nd	nd	nd
33	41	13	30	93	nd	122	78	nd	140
34	16	3	nd	15	nd	61	nd	nd	126
35	14	nd	nd	8	74	91	49	397	nd
36	11	nd	9	11	nd	38	nd	46	nd
37	nd	nd	nd	nd	27	84	nd	nd	60
38	7	nd	nd	16	23	112	44	81	nd
39	11	nd	11	nd	69	87	nd	7	nd
40	6	nd	nd	nd	nd	123	nd	26	54
41	6	nd	9	18	18	46	43	661	nd
42	2	2	9	nd	30	nd	nd	302	82
43	2	nd	nd	28	nd	nd	nd	177	94
44	10	nd	13	22	nd	79	nd	60	65
45	4	58	nd	nd	27	nd	nd	282	nd
46	nd	nd	nd	nd	47	nd	nd	942	63
48	11	nd	nd	11	nd	68	39	83	nd
49	21	nd	nd	12	nd	50	82	23	92
50	23	nd	nd	47	nd	233	nd	75	11830
51	2	nd	nd	nd	nd	79	nd	108	161
52	15	nd	8	nd	44	100	nd	76	nd
53	6	2	nd	19	nd	nd	nd	89	152
54	4	nd	12	19	nd	61	133	nd	74

5. STATISTICAL ANALYSIS OF DATA

5.1. GOAL OF THE STATISTICAL ANALYSIS

A statistical analysis program called SPSSX [32] was used to find correlations among the samples through the study of the trace element composition of each. Because rhyolites taken from the same quarry would have formed in the same way and been exposed to identical metamorphic processes before they were fashioned into tools, trace element composition of those stones should be about the same. Groups and associations formed from the statistical analysis should therefore assist in the identification of stones which came from the same source.

5.2. CLUSTER ANALYSIS

The method of cluster analysis is a statistical technique which uses a variety of attributes to identify similarities and differences among objects to form groups of like attributes [32]. A relative measure of how alike or dissimilar objects are may be obtained from the statistical concept of the squared Euclidean distance, in which the square of the numerical attributes of two objects are summed together. An example of this would be to calculate the differences in the concentrations of the trace elements of two rhyolite samples, square those differences and then add them together. Comparing the result with the squared distances between other pairs of samples provides a way of determining which stones came from the same source.

One such method, agglomerative hierarchical cluster analysis, was used to analyze the spectral data and form groups which may have come from the same source. This method begins with all 51 rhyolite samples as separate cases, then forms clusters of the cases which seem the most alike in the succeeding steps. The process continues, adding individual cases to specific clusters and combining clusters, until a single cluster is formed of all 51 samples.

5.3. RESULTS OF THE CLUSTER ANALYSIS

Two cluster analyses of the samples were performed using the 10 trace elements shown in Table II to derive the clustering variables. In one analysis, the absolute concentrations calculated by PIXAN were used as the clustering variables; and in the other analysis, ratios of the concentrations of each element to that of iron were used. The purpose of the second approach was to investigate the effects of possible uncertainties in the charge integration, which would have affected the calculation of the absolute concentrations by the program THICK.

Some results of the cluster analysis are illustrated in Figure 14, where a circle represents a cluster and the numbers within it represent the samples belonging to that cluster. The circles on the left-hand side of the figure show three clusters formed using the absolute concentrations as the clustering variables; those on the right-hand side show similar clusters formed using the ratios of elemental concentrations to the concentration of iron. As is evident from Figure 14, the two approaches yielded slightly different cluster memberships. However, many samples were found to be common to clusters formed using the two approaches. In some sense, the similarities between samples found in the intersections of the circles are independent of the clustering method used. The samples in the intersections were therefore treated as the members of clusters formed using a "combined" method.

Table IV and Figure 15 show the mean values of the elemental concentrations of the samples in the three clusters found. Many of these concentrations for a given element are equal, within statistical uncertainties, for the three clusters. Several, however, are not, and illustrate the chemical basis for the distinctions between the clusters. For example, Cluster A contains the most Fe and Y, but the least K, Rb, Sr, and Ba. Cluster C, on the other hand, contains the most K, Rb, Sr, and Ba, but the least Fe and Y. The only

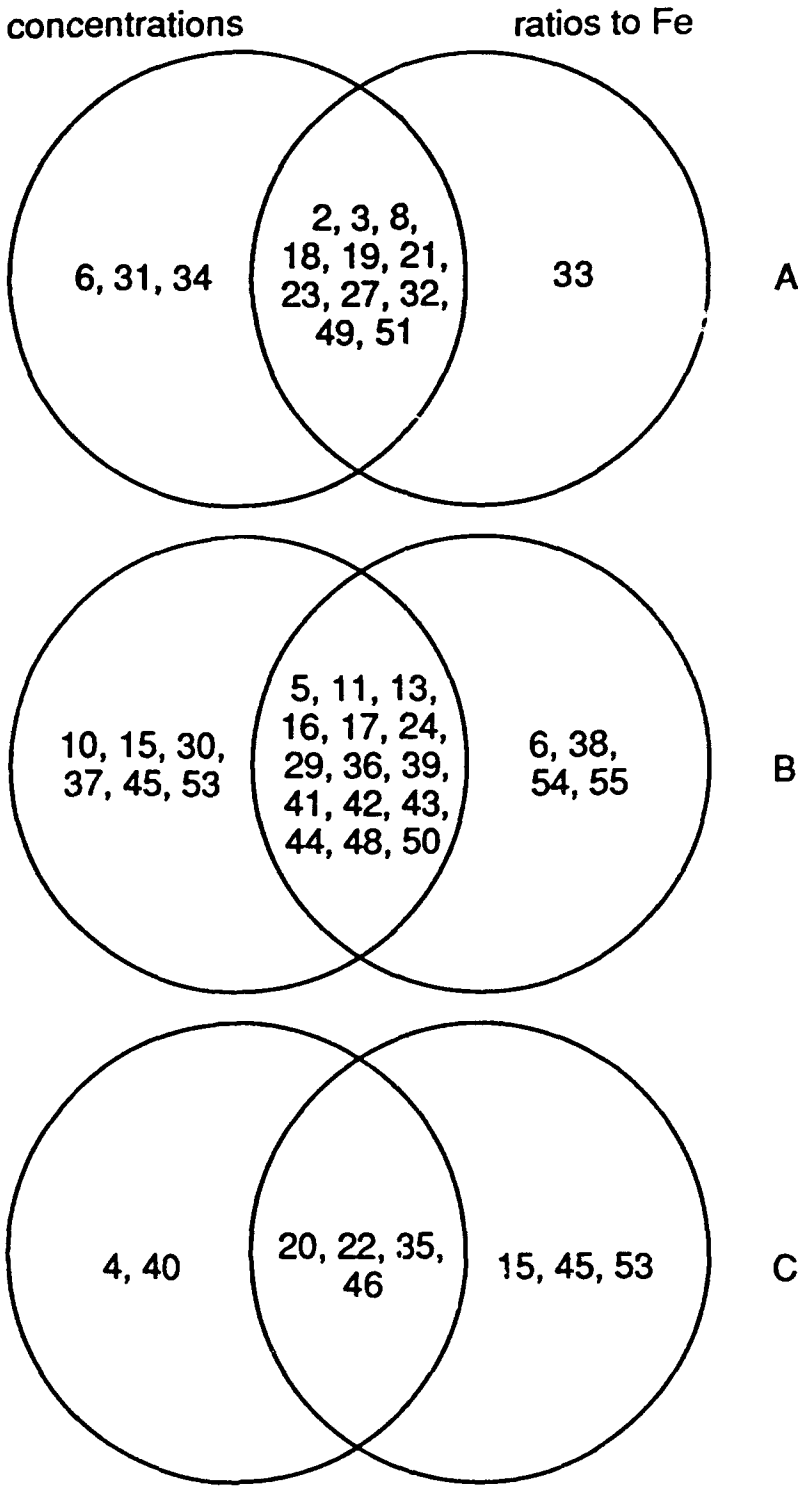

Figure 14. Cluster memberships. Each pair of circles represents a set of samples found to be similar by the cluster analysis. The left-hand circle in each pair represents the results of clustering by concentrations; the right-hand circle, the results of clustering by ratios of the concentration of each element in a sample to that of Fe.

distinguishing characteristic of Cluster B seems to be that its samples contain the most Pb. It is satisfying to observe that the concentrations of chemically-similar pairs of elements, such as K and Rb, on the one hand, and Sr and Ba, on the other, are observed to be correlated within the clusters. This might be expected in any reasonable model of stone formation.

The largest differences in concentration are observed for K and Rb, for which the ratio of concentrations in Cluster C to those in Cluster A are on the order of 2:1. These differences are large compared to those that might be expected to occur due to sample nonuniformities or uncertainties in charge collection.

Table IV. Average concentrations (parts per million, by weight) of ten elements in the clusters A, B, and C. Cluster membership was determined by the combined method. Quoted uncertainties represent the standard deviations of the concentrations within each cluster.

	Cluster A	Cluster B	Cluster C
Fe	15732 ± 2839	13625 ± 1860	11681 ± 818
K	25013 ± 3674	34530 ± 3286	47176 ± 4586
Ca	2316 ± 2125	1228 ± 667	1710 ± 1161
Ti	793 ± 270	725 ± 244	839 ± 231
Mn	271 ± 129	266 ± 114	350 ± 271
Cu	26 ± 30	17 ± 8	28 ± 8
Zn	60 ± 11	122 ± 146	80 ± 46
Ga	33 ± 6	30 ± 9	29 ± 12
Rb	61 ± 26	95 ± 31	131 ± 17
Zr	685 ± 346	560 ± 156	572 ± 301

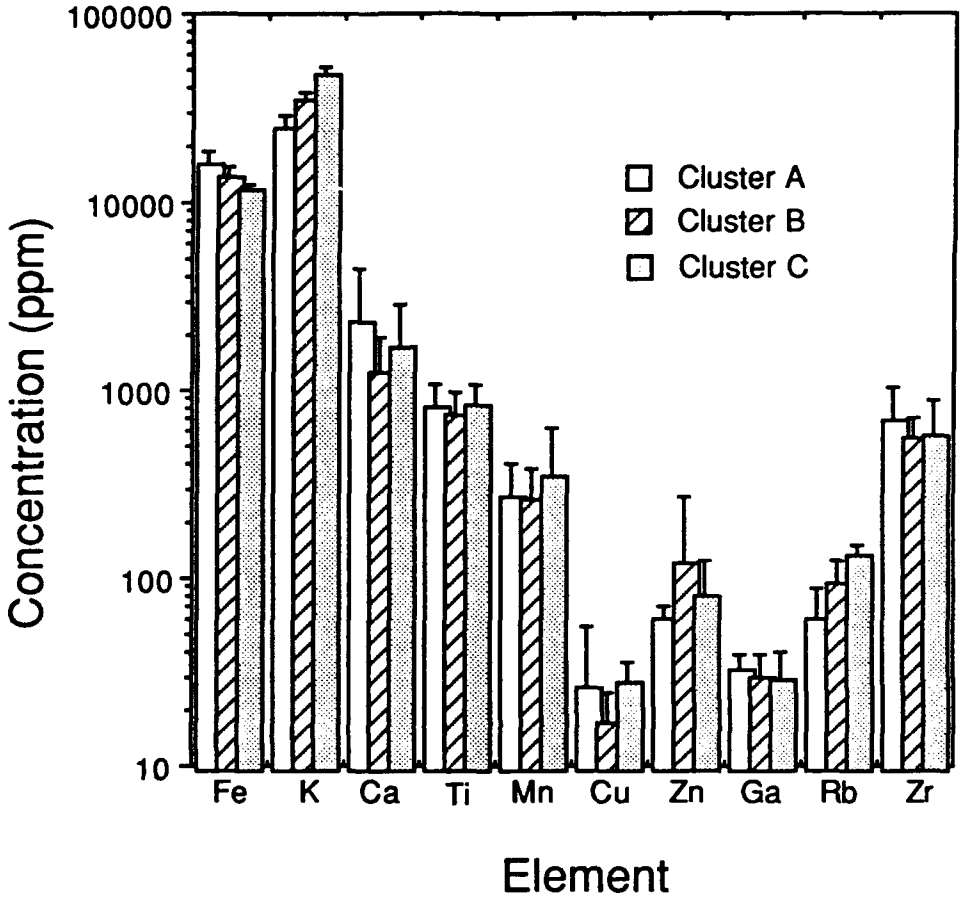

Figure 15. Average elemental compositions of the samples in clusters A, B, and C. Cluster membership was determined using the combined method. Error bars represent the standard deviations of the compositions within each sample.

6. SUMMARY AND CONCLUSIONS

6.1. IBA DEVELOPMENT

The primary concern of this project was to develop the necessary techniques for studying the rhyolite stone tools provided by the Maryland Historical Trust. Calibration of the beam energy with the $^{27}Al(p,\gamma)^{28}Si$ resonance provided a precision in the value of the beam energy on target which had not been previously known. Implementation of a Si(Li) detector and a 0.025-mm Al filter provided greater resolution and better sensitivity to the heavier trace elements representing less than 5% of the composition. Installation of the PIXAN code on the VAX computer and the addition of routines to calculate the transmission coefficient of air and the Al filter made analysis of the spectra more efficient and more accurate.

6.2. PIXE RESULTS

Ten elements with concentrations ranging from approximately 10 ppm in the case of Cu to about 5% by weight for Fe were detected in almost all samples Additionally, nine other elements were detected in several of the samples. Expected correlations were observed between concentrations of chemically-similar elements in the samples. This indicates that in-air PIXE is a viable technique for studying the elemental compositions of rhyolites.

6.3. ARCHEOLOGICAL IMPLICATIONS

Though this exploratory study was intended to develop ion beam analysis methods tailored specifically to the further study of trace elemental analyses of rhyolites, considerable archeological implications are evident at this point. While specific rhyolite sources were not identified, the results of cluster analyses, combined with the discovery of an iron tradestone among the rhyolite tools provide a new perspective on the previously

unknown extent of trade and exchange during the Selby Bay Phase. The data compiled through this study suggest that the social conditions during this epoch supported a complex and broad-based trade and exchange network.

Inspection of the concentration data in Table II indicates that the absolute elemental concentrations of stones from the same geographic area vary considerably and patterns of concentration ratios similarly seem to indicate more diversity than similarity of stones found at particular sites. The cluster analyses described above supports this diversity, because the stones do not cluster to specific sites, instead clustering occurs in a more complex way. This diversity suggests that the points found in at any particular site did not come from the same rhyolite source. The presence of rhyolites from several different sources at one site challenges the theory that rhyolite-retrieving task groups were sent into the mountains by communities in southern Maryland. The diversity suggests, instead, that the trade and exchange network was a more likely means of procuring rhyolites for groups who lived far from the aboriginal quarries of the Blue Ridge Mountains.

Evidence of geographic distinction between two of the groups developed through cluster analysis further supports trade as the probable means of obtaining rhyolites. The common members of Cluster A, shown in Figure 14, were found in sites along the Patuxent River, at the Patuxent Point site, and in the Susquehanna River estuary. The members of Cluster C, on the other hand, were located at sites along the Patuxent River, at Patuxent Point, and along the Potomac River. The location of the Patuxent Point site at the mouth of one river and between the two other rivers makes it ideally situated for use as a trading center, as would be implied by the presence of artifacts from the sources represented by clusters A and B at the Patuxent River and Patuxent Point sites. Additionally, while these groups share the common areas of the Patuxent River and Patuxent Point, the exclusion of one of the other rivers in a group indicates a distinction between trade to the north of the Patuxent Point site and trade further south. This supports

the picture of a broad-based trade network which filtered rhyolites down the rivers from the mountains to the Bay area.

The most dramatic evidence of a far-reaching trade network, however, is provided by the discovery of an iron tradestone at the Patuxent Point site. An extremely high concentration of iron in one sample was apparent during data collection due to the overwhelming iron peak and lack of any other features in the spectrum. Later, visual analysis by Dr. Michael Stewart, an expert on prehistoric trade on the Delmarva Peninsula, confirmed that this stone was not rhyolite at all, but was, instead, an iron tradestone characteristic of the tradestones found in northern Delaware [10]. While trade with Maryland's Eastern Shore is evident in the appearance of chert on the western shore of the Chesapeake, and accounted for in the folklore of the Native Americans of southern Maryland, previous studies in this area had not produced evidence of the iron tradestones which were indigenous to the northern Delmarva Peninsula. This unique link to Delaware and the Delmarva peninsula suggests that the trade and exchange networks of the Selby Bay Phase were complex and extensive; a further indication of broad-based exchange in the society at that time.

The results of trace element concentration comparisons and cluster analysis suggest that elaborate broad-based trade networks were established in the Middle Woodland Selby Bay Phase. Diversity of rhyolite sources at each site, evident from the varying elemental composition of tools found at the sites, indicates that trade and exchange provided the prehistoric people of southern Maryland with projectile points fashioned from rhyolite. Evidence of a north-south trade difference centered at the Patuxent Point site suggests that waterways were the avenues of trade and that extensive and complex exchange networks relied on these waterways. Presence of an iron tradestone from the northern Delmarva Peninsula is further testimony to the extent of the trade networks, and suggests a link with the Eastern Shore that had been previously suspected, but not confirmed.

REFERENCES

[1] M. Meyer and G. Demortier, Nuclear Instruments and Methods in Physics Research B49 (1990) 300-304.

[2] S.J. Fleming, C.P Swann, P.E. McGovern and L. Horne, Nuclear Instruments and Methods in Physics Research B49 (1990) 293-299.

[3] U. Lindh, H. Mutvei, T. Sunde and T. Westermark, Nuclear Instruments and Methods in Physics Research B30 (1988) 388-392.

[4] M. Peisach, Nuclear Instruments and Methods in Physics Research B14 (1986) 99-115.

[5] S.A. Reeve, J. Russo, D.H. Pogue and J.M. Herbert, An Archeological and Historical Survey of Myrtle Point, St. Mary's County, Maryland, Jefferson Patterson Park and Museum, Occasional Papers No. 3 (1989).

[6] Dr. S.A. Reeve (private communication).

[7] R.M. Stewart, Archaeology of Eastern North America 15 (1987) 47-57.

[8] R.M. Stewart, in: University of Delaware Center for Archaeological Research Monograph No. 3, ed. Jay F. Custer (University of Delaware 1984), 2-13.

[9] R.M. Stewart, Archaeology of Eastern North America 17 (1989) 47-78.

[10] J.F. Custer, Prehistoric Cultures of the Delmarva Peninsula (University of Delaware Press 1989), 185-249.

[11] Curtiss Peterson (private communication).

[12] P.A. Tipler, Modern Physics (Worth Publishers 1987), p. 153.

[13] G. Amsel, Ch. Heitz and M. Menu, Nuclear Instruments and Methods in Physics Research B14 (1986) 34.

[14] D.D. Cohen, Nuclear Instruments and Methods in Physics Research B49 (1990) 1-9.

[15] F. Folkmann, C. Gaarde, T. Huus and K.Kemp, Nuclear Instruments and Methods in Physics Research 116 (1974) 487-499.

[16] C.P. Swann and S.J. Fleming, Scanning Microscopy, Vol. 2, No. 1 (1988) 197-207.

[17] E. Clayton, PIXAN: The Lucas Heights PIXE Analysis Computer Package (1986).

[18] W. Chu, J. W. Mayer and M.A. Nicolet, Backscattering Spectrometry, (Academic Press, Inc., 1978), p. 23.

[19] S.A.E. Johansson and J.L. Campbell, PIXE: A Novel Technique for Elemental Analysis (John Wiley & Sons Ltd. 1988), p. 2.

[20] M. Peisach, C.A. Pineda and L. Jacobsen, Nuclear Instruments and Methods in Physics Research B49 (1990) 309-312.

[21] P. Duerden, J.R. Bird, M.D. Scott, E. Clayton, L.H. Russel and D.D. Cohen, Nuclear Instruments and Methods 168 (1980) 447-452.

[22] T.A. Cahill, Annual Review of Nuclear Particle Science 30 (1980) 211-252.

[23] National Electrostatics Corporation Instruction Manual for Operation & Service Charge Exchange RF Source.

[24] R.J. Girnius and L. W. Anderson, Nuclear Instruments and Methods 137 (1976) 376.

[25] National Electrostatics Corporation Instruction Manual for Installation and Service of the 5SDH Pelletron Accelerator.

[26] J.J. Campbell, Nuclear Instruments and Methods in Physics Research B49 (1990) 115-125.

[27] EG&G Ortec, Solid-State Photon Detector Operators Manual: SLP Series Lithium-Drifted Silicon Low-Energy Photon Spectrometer.

[28] P. Duerden, D.D. Cohen, E. Clayton, J.R. Bird, W.R. Ambrose and B.F. Leach, Analytical Chemistry vol. 51, no. 14 (1979) 2350-2354.

[29] C.P. Swann and S.J. Fleming, Nuclear Instruments and Methods in Physics Research B41 (1986) 61-69.

[30] W.J. Veigele, Atomic Data, Vol 5, No. 1 (1973) 51-111.

[31] FIXPIX is a PASCAL computer program written by David Clipsham, USNA Class of 1990.

[32] SPSSX User's Guide, (SPSS, Inc. 1986).

GLOSSARY

Background - Radiation from sources other than the source being measured.

Bremsstrahlung - Continuous radiation emitted when a charged particle is accelerated.

Coulomb barrier - The Coulomb repulsion that tends to keep positively charged bombarding particles from entering the nucleus.

Cross section - A measure of the probability of a reaction's occurring.

Electron-hole pair production - A process in which an electron is stripped from the valence band of a semiconductor and is promoted to the conduction band. This process allows current to flow easily through the semiconductor.

Fluorescence yield - The ratio of radiative electron energy level transitions to radiationless (Auger) transitions.

FWHM (Full Width at Half Maximum) - A measure of the "sharpness" of a peak, where the width is measured at a height equal to half the amplitude or maximum height of the peak.

Knapping - A process in which stone tools are formed by breaking off parts of the raw stone until a shaped, sharp-edged tool is produced.

MCA (Multi-Channel Analyzer) - A program which creates histograms of data. In this case, the histogram was a plot of the number of counts of X rays in a particular energy channel.

Rhyolite - Also known as Metarhyolite, this is a light-colored volcanic rock composed primarily of silicon and feldspar. Found locally in the Blue Ridge Mountains of Maryland and Pennsylvania.

Secondary electron - An electron ejected from an atom as a result of bombardment by an ion.